

Equation of state of hadron resonance gas and the phase diagram of strongly interacting matter

L.M. Satarov,^{1,2} M.N. Dmitriev,² and I.N. Mishustin^{1,2}

¹*Frankfurt Institute for Advanced Studies,*

J.W. Goethe University, D-60438 Frankfurt am Main, Germany

²*The Kurchatov Institute, Russian Research Center, 123182 Moscow, Russia*

Abstract

The equation of state of hadron resonance gas at finite temperature and baryon density is calculated taking into account finite-size effects within the excluded volume model. Contributions of known hadrons with masses up to 2 GeV are included in the zero-width approximation. Special attention is paid to the role of strange hadrons in the system with zero total strangeness. A density-dependent mean field is added to guarantee that the nuclear matter has a saturation point and a liquid-gas phase transition. The deconfined phase is described by the bag model with lowest order perturbative corrections. The phase transition boundaries are found by using the Gibbs conditions with the strangeness neutrality constraint. The sensitivity of the phase diagram to the hadronic excluded volume and to the parametrization of the mean-field is investigated. The possibility of strangeness-antistrangeness separation in the mixed phase is analyzed. It is demonstrated that the peaks in the K/π and Λ/π excitation functions observed at low SPS energies can be explained by a nonmonotonous behavior of the strangeness fugacity along the chemical freeze-out line.

PACS numbers: 21.65.Mn, 21.65.Qr, 24.85.+p, 25.75.Nq

I. INTRODUCTION

Relativistic heavy-ion collisions represent a powerful tool for studying properties of strongly interacting matter in the laboratory. The main goal is to explore the phase diagram of such matter and, in particular, to investigate properties of a new phase – the quark-gluon plasma (QGP). This can be done only indirectly, i.e. by comparing predictions of different theoretical models with experimental data. The fluid-dynamical model is one of the most popular models for describing the relativistic heavy-ion collisions. In this model one needs the equation of state (EOS) and transport coefficients as input information. The QCD lattice calculations can give reliable results on thermodynamic properties of strongly interacting matter only for small baryon chemical potentials. In this case a crossover type of the deconfinement transition is predicted [1]. It seems that this prediction is confirmed by recent RHIC experiments (see e.g. [2]). The structure of the phase diagram at high baryon densities remains rather uncertain [3]. However, exactly the baryon-rich matter attracts the main interest due to the possibility of the first order deconfinement phase transition [4, 5]. The future facility for antiproton and ion research (FAIR) at GSI (Darmstadt) is especially focused on heavy-ion collisions with bombarding energies 20-40 AGeV, where maximal baryon densities of about 10 times the normal nuclear density $n_0 = 0.15 \text{ fm}^{-3}$ are expected [6]. Some interesting results concerning dense baryon matter have been obtained already at low SPS energies by the NA49 Collaboration [7, 8].

To understand properties of the deconfinement transition, one needs to know accurately the EOS of the hadronic as well as the quark-gluon phases. As demonstrated in Ref. [9], very often arbitrarily chosen models for these two phases do not lead to any phase transition. For instance, taking an ideal resonance gas for the hadronic phase and the bag model for the QGP, one comes to the paradoxical conclusion that the hadronic phase is thermodynamically stable at high temperatures [10]. It is clear that at high densities the repulsive interaction between hadrons becomes important and should be explicitly taken into account. One can introduce such interaction via the vector meson exchange as done in the relativistic mean-field models of the Walecka type [11]. However, the repulsive vector field in these models is proportional to the net baryon density and, therefore, can not solve the problem in the case of baryon-free matter. Another possibility is to take into account the finite size of hadrons within the Van der Waals approach [12]. Different versions of

the EOS of strongly interacting matter with finite-size corrections have been considered in Refs. [13, 14, 15, 16, 17, 18, 19], but the sensitivity of the phase diagram to the choice of hadronic volumes was not fully investigated. In this paper we address this problem on the quantitative level. This allows us to derive a consistent EOS with the deconfinement phase transition. We also study the role of the strangeness neutrality constraint, which previously has been investigated only qualitatively [20, 21].

The paper is organized as follows. In Sect. II we describe thermodynamic properties of a hadron resonance gas in the excluded volume approximation. In this section we show that the strangeness neutrality constraint leads to a non-monotonic behavior of the K/π and Λ/π multiplicity ratios along the freeze-out line in the chemical potential-temperature plane. The bag model for a quark-gluon phase is formulated in Sect. III. The phase diagram of strongly interacting matter is studied in Sect. IV. In particular, we investigate its sensitivity to the choice of hadronic volumes. In Sect. V we introduce the mean-field interaction of baryons in order to implement the liquid-gas phase transition in nuclear matter at low temperatures. In Sect. VI we summarize our results and outline possible improvements of the model.

II. HADRONIC PHASE

A. Hadron resonance gas within the excluded volume approximation

Let us consider a purely hadronic system in the total volume V assuming local thermodynamic equilibrium and neglecting the isospin, Coulomb and surface effects. Since hadrons are composite particles, their finite sizes should be taken into account at high enough densities or temperatures. The intuitive way to implement the finite-size effects is to use the Van der Waals prescription which is known also as the excluded volume approximation. Within such an approach the hadronic system is still regarded as an ideal gas, but in the volume reduced by the volume occupied by constituents,

$$V' = V - \sum_i v_i N_i. \quad (1)$$

Here v_i and N_i are the excluded volume and the number of hadrons of type i , the sum runs over all hadronic species i . In the following we assume that all hadrons have the same

radius r_h . Then one can estimate the excluded volume per particle as 1/2 of a spherical volume with the radius $2r_h$ [12]

$$v_i = v = \frac{16\pi}{3} r_h^3. \quad (2)$$

This approximation should be good enough at particle densities much smaller than the density of close packing [56]. The quantity v will be considered below as a model parameter. According to the analysis of hadronic yields observed in relativistic heavy-ion collisions [18], the reasonable interval of hadronic radii is $r_h \simeq (0.3 - 0.6)$ fm. This corresponds to the excluded volume range $v \simeq (0.5 - 3)$ fm³.

Making the replacement $V \rightarrow V'$ in the canonical partition sum, one obtains the following equation for the pressure of hadronic system [16]

$$P = \sum_i P_i(\tilde{\mu}_i, T), \quad (3)$$

where $P_i(\tilde{\mu}_i, T)$ is the partial pressure of ideal gas of i -th hadrons at temperature T and chemical potential $\tilde{\mu}_i$. The relation connecting $\tilde{\mu}_i$ with the real chemical potential μ_i reads

$$\tilde{\mu}_i = \mu_i - vP. \quad (4)$$

In fact, Eqs. (3)–(4) give the integral equation for P at a given temperature and set of chemical potentials $\{\mu_i\}$. In the limiting case $v \rightarrow 0$ one obtains the Dalton law for a mixture of ideal gases of different hadrons.

The condition of chemical equilibrium with respect to strong interactions leads to the relations

$$\mu_i = B_i \mu + S_i \mu_S, \quad (5)$$

where $B_i = 0, \pm 1$ and $S_i = 0, \pm 1, \pm 2 \dots$ are, respectively, the baryon and strangeness quantum numbers of the i -th hadronic species, μ and μ_S denote the baryon and strange chemical potentials. Therefore, pressure of a chemically equilibrated system is a function of only three independent variables μ, μ_S, T :

$$P = P(\mu, \mu_S, T). \quad (6)$$

This function satisfies the thermodynamic relation [12]

$$dP = s dT + n d\mu + n_S d\mu_S, \quad (7)$$

where s is the entropy density, n and n_S are, respectively, the baryon and strangeness number densities. In this paper we consider only the hadronic matter with zero net strangeness. Such matter may be created e.g. in collisions of nonstrange projectile and target nuclei. Since strangeness is conserved in strong interactions, the produced system must obey the condition of strangeness neutrality

$$n_S(\mu, \mu_S, T) = 0. \quad (8)$$

In a baryon-asymmetric matter ($\mu \neq 0$) this condition can be satisfied only at nonzero strange chemical potential μ_S . It is easy to show that μ_S should be positive in the baryon-rich matter. This follows from the fact that the negative strangeness is carried by hyperons while the positive strangeness is associated mostly with kaons.

From Eqs. (3)–(5), and (7), one can obtain explicit relations for thermodynamic quantities s, n, n_S [18]:

$$s = \frac{\partial P}{\partial T} = r \sum_i \tilde{s}_i(\tilde{\mu}_i, T), \quad (9)$$

$$n = \frac{\partial P}{\partial \mu} = r \sum_i B_i \tilde{n}_i(\tilde{\mu}_i, T), \quad (10)$$

$$n_S = \frac{\partial P}{\partial \mu_S} = r \sum_i S_i \tilde{n}_i(\tilde{\mu}_i, T), \quad (11)$$

where $\tilde{s}_i = \partial P_i / \partial T$ and $\tilde{n}_i = \partial P_i / \partial \tilde{\mu}_i$ are, respectively, the entropy and particle number density of the ideal gas of i -th hadrons. The reduction factor r in r.h.s of Eqs. (9)–(11) is defined as

$$r = (1 + v \sum_i \tilde{n}_i)^{-1}. \quad (12)$$

The number density of the i -th species satisfies the relations

$$n_i = \frac{\partial P}{\partial \mu_i} = r \tilde{n}_i \leq \frac{1}{v}. \quad (13)$$

By using Eqs. (3)–(5), (9)–(12) and the Gibbs–Duhem equation

$$\epsilon = -P + Ts + \mu n + \mu_S n_S, \quad (14)$$

one obtains the expression for energy density

$$\epsilon = r \sum_i \tilde{\epsilon}_i(\tilde{\mu}_i, T), \quad (15)$$

where $\tilde{\epsilon}_i = -P_i + T\tilde{s}_i + \tilde{\mu}_i\tilde{n}_i$ is energy density of the ideal gas of i -th hadrons. Below we take into account the contributions of stable hadrons as well as mesonic and baryonic resonances in the zero-width approximation. In the grand canonical ensemble the thermodynamic functions of the relativistic ideal gas of species i are given by the following explicit relations ($\hbar = c = 1$)

$$\begin{pmatrix} \tilde{\epsilon}_i \\ P_i \\ \tilde{n}_i \end{pmatrix} = \frac{g_i}{2\pi^2} \int_{m_i}^{\infty} d\epsilon \frac{\sqrt{\epsilon^2 - m_i^2}}{\exp\left(\frac{\epsilon - \tilde{\mu}_i}{T}\right) \pm 1} \begin{pmatrix} \epsilon^2 \\ \frac{1}{3}(\epsilon^2 - m_i^2) \\ \epsilon \end{pmatrix}, \quad (16)$$

where m_i is the mass of the i -th hadron and g_i is its spin–isospin degeneracy factor. The lower sign in r.h.s. of (16) corresponds to mesons ($B_i = 0$) [57] and the upper one, to baryons ($B_i = 1$) or antibaryons ($B_i = -1$). The integrals in Eq. (16) are calculated numerically as explained in Appendix.

In the present work we include contributions of the lightest hadrons with masses $m_i \lesssim 2$ GeV. Altogether we take into account 59 mesonic and 41 baryonic species listed in Ref. [22]. This corresponds to 307 different isospin states of mesons, baryons and antibaryons. Characteristics of hadrons included in our calculations are given in Table I. For hadrons with nonzero isospin we use the isospin averaged mass values. Note, that unless otherwise stated, we do not include a very broad scalar meson resonance $f_0(600)$ with mass $m \sim 0.6$ GeV and width $\Gamma \gtrsim 0.6$ GeV [58]. The last two columns of Table I give the average numbers of pions (d_i^π) and kaons (d_i^K) produced in decays of the i -th hadron. These numbers are calculated by using the decay branching ratios from Ref. [22] [59]. For particles, stable with respect to strong interactions, we use the values $d_i^\pi = d_i^K = 0$. In decays of heavy hyperons only \overline{K} -mesons, not kaons, are produced. In these cases the last column of Table I gives the contributions of corresponding antihyperons (see entries with asterisks). For example, in the case $i = \Omega^-$ one has $d_\Omega^K = 0$, $d_\Omega^{\overline{K}} \simeq 0.68$.

B. Thermodynamic properties of hadronic phase

Below we present numerical results for a nonstrange ($n_S = 0$), isospin-symmetric hadronic matter. Figure 1 shows pressure P as a function of T for different values of μ . One can see that the excluded volume corrections (EVC) reduce the pressure as compared to the calculation with $v = 0$. The difference between two calculations increases with raising T

TABLE I: Characteristics of hadronic species included in the calculation ^a.

| hadron | m_i (GeV) | g_i | B_i | S_i | I_i | d_i^π | d_i^K | hadron | m_i (GeV) | g_i | B_i | S_i | I_i | d_i^π | d_i^K |
|-------------------|-------------|-------|-------|-------|-------|-----------|---------|---------------------|-------------|-------|-------|-------|-------|-----------|---------|
| π | 0.140 | 3 | 0 | 0 | 1 | 1 | 0 | $N(1535)$ | 1.530 | 4 | 1 | 0 | 1/2 | 1.45 | 0 |
| K | 0.496 | 2 | 0 | 1 | 1/2 | 0 | 1 | $\pi_1(1600)$ | 1.596 | 9 | 0 | 0 | 1 | 3.54 | 0.03 |
| \bar{K} | 0.496 | 2 | 0 | -1 | 1/2 | 0 | 0 | $\Delta(1600)$ | 1.600 | 16 | 1 | 0 | 3/2 | 1.93 | 0 |
| η | 0.543 | 1 | 0 | 0 | 0 | 1.95 | 0 | $\Lambda(1600)$ | 1.600 | 2 | 1 | -1 | 0 | 0.6 | 0.4* |
| ρ | 0.776 | 9 | 0 | 0 | 1 | 2 | 0 | $\Delta(1620)$ | 1.630 | 8 | 1 | 0 | 3/2 | 1.75 | 0 |
| ω | 0.782 | 3 | 0 | 0 | 0 | 2.79 | 0 | $\eta_2(1645)$ | 1.617 | 5 | 0 | 0 | 0 | 3.24 | 0.1 |
| K^* | 0.892 | 6 | 0 | 1 | 1/2 | 1 | 1 | $N(1650)$ | 1.655 | 4 | 1 | 0 | 1/2 | 1.2 | 0.07 |
| \bar{K}^* | 0.892 | 6 | 0 | -1 | 1/2 | 1 | 0 | $\omega(1650)$ | 1.670 | 3 | 0 | 0 | 0 | 4.18 | 0 |
| N | 0.939 | 4 | 1 | 0 | 1/2 | 0 | 0 | $\Sigma(1660)$ | 1.660 | 6 | 1 | -1 | 1 | 0.8 | 0.2* |
| η' | 0.958 | 1 | 0 | 0 | 0 | 3.25 | 0 | $\Lambda(1670)$ | 1.670 | 2 | 1 | -1 | 0 | 0.89 | 0.3* |
| f_0 | 0.980 | 1 | 0 | 0 | 0 | 2.95 | 0 | $\Sigma(1670)$ | 1.670 | 2 | 1 | -1 | 1 | 1.25 | 0 |
| a_0 | 0.980 | 3 | 0 | 0 | 1 | 2.95 | 0.15 | $\omega_3(1670)$ | 1.667 | 7 | 0 | 0 | 0 | 3.90 | 0 |
| ϕ | 1.020 | 3 | 0 | 0 | 0 | 0.48 | 0.83 | $\pi_2(1670)$ | 1.672 | 15 | 0 | 0 | 1 | 3.90 | 0.04 |
| Λ | 1.116 | 2 | 1 | -1 | 0 | 0 | 0 | Ω^- | 1.672 | 4 | 1 | -3 | 0 | 0.32 | 0.68* |
| h_1 | 1.170 | 3 | 0 | 0 | 1 | 3 | 0 | $N(1675)$ | 1.675 | 12 | 1 | 0 | 1/2 | 1.6 | 0 |
| Σ | 1.189 | 6 | 1 | -1 | 1 | 0 | 0 | $\phi(1680)$ | 1.680 | 3 | 0 | 0 | 0 | 1 | 0.5 |
| a_1 | 1.230 | 9 | 0 | 0 | 1 | 3 | 0 | $K^*(1680)$ | 1.717 | 6 | 0 | 1 | 1/2 | 1.61 | 1 |
| b_1 | 1.230 | 9 | 0 | 0 | 1 | 3.79 | 0 | $\bar{K}^*(1680)$ | 1.717 | 6 | 0 | -1 | 1/2 | 1.61 | 0 |
| Δ | 1.232 | 16 | 1 | 0 | 3/2 | 1 | 0 | $N(1680)$ | 1.685 | 12 | 1 | 0 | 1/2 | 1.35 | 0 |
| f_2 | 1.270 | 5 | 0 | 0 | 0 | 2.20 | 0.05 | $\rho_3(1690)$ | 1.688 | 21 | 0 | 0 | 1 | 3.35 | 0.05 |
| K_1 | 1.273 | 6 | 0 | 1 | 1/2 | 2.12 | 1 | $\Lambda(1690)$ | 1.690 | 4 | 1 | -1 | 0 | 1.2 | 0.25* |
| \bar{K}_1 | 1.273 | 6 | 0 | -1 | 1/2 | 2.12 | 0 | $\Xi(1690)$ | 1.690 | 8 | 1 | -2 | 1/2 | 0.33 | 0.66* |
| f_1 | 1.285 | 3 | 0 | 0 | 1 | 3.69 | 0.09 | $\rho(1700)$ | 1.720 | 9 | 0 | 0 | 1 | 4 | 0 |
| $\eta(1295)$ | 1.295 | 1 | 0 | 0 | 0 | 3.95 | 0 | $N(1700)$ | 1.700 | 8 | 1 | 0 | 1/2 | 1.9 | 0 |
| $\pi(1300)$ | 1.300 | 3 | 0 | 0 | 1 | 3 | 0 | $\Delta(1700)$ | 1.700 | 16 | 1 | 0 | 3/2 | 1.85 | 0 |
| Ξ | 1.315 | 4 | 1 | -2 | 1/2 | 0 | 0 | $N(1710)$ | 1.710 | 4 | 1 | 0 | 1/2 | 1.65 | 0.15 |
| a_2 | 1.318 | 15 | 0 | 0 | 1 | 3.04 | 0.05 | $f_0(1710)$ | 1.714 | 1 | 0 | 0 | 0 | 2.87 | 0.25 |
| $f_0(1370)$ | 1.370 | 1 | 0 | 0 | 1 | 2 | 0 | $N(1720)$ | 1.720 | 8 | 1 | 0 | 1/2 | 1.71 | 0.07 |
| $\Sigma(1385)$ | 1.385 | 12 | 1 | -1 | 1 | 1 | 0 | $\Sigma(1750)$ | 1.750 | 6 | 1 | -1 | 1 | 1.12 | 0.4* |
| $K_1(1400)$ | 1.400 | 6 | 0 | 1 | 1/2 | 1.97 | 1 | $K_2(1770)$ | 1.773 | 10 | 0 | 1 | 1/2 | 2.65 | 1 |
| $\bar{K}_1(1400)$ | 1.400 | 6 | 0 | -1 | 1/2 | 1.97 | 0 | $\bar{K}_2(1770)$ | 1.773 | 10 | 0 | -1 | 1/2 | 2.65 | 0 |
| $\eta(1405)$ | 1.405 | 1 | 0 | 0 | 0 | 2.59 | 0.3 | $\Sigma(1775)$ | 1.775 | 18 | 1 | -1 | 1 | 1.58 | 0.45* |
| $\Lambda(1405)$ | 1.406 | 2 | 1 | -1 | 0 | 1 | 0 | $K_3^*(1780)$ | 1.776 | 14 | 0 | 1 | 1/2 | 1.79 | 1 |
| $K^*(1410)$ | 1.414 | 6 | 0 | 1 | 1/2 | 1.54 | 1 | $\bar{K}_3^*(1780)$ | 1.776 | 14 | 0 | -1 | 1/2 | 1.79 | 0 |
| $\bar{K}^*(1410)$ | 1.414 | 6 | 0 | -1 | 1/2 | 1.54 | 0 | $\pi(1800)$ | 1.812 | 3 | 0 | 0 | 1 | 3.76 | 0.25 |
| $f_1(1420)$ | 1.420 | 3 | 0 | 0 | 1 | 1 | 0 | $\Lambda(1800)$ | 1.800 | 2 | 1 | -1 | 0 | 0.92 | 0.54* |
| $\omega(1420)$ | 1.420 | 3 | 0 | 0 | 0 | 3 | 0 | $\Lambda(1810)$ | 1.810 | 2 | 1 | -1 | 0 | 0.65 | 0.75* |
| K_0^* | 1.425 | 2 | 0 | 1 | 1/2 | 0.93 | 1 | $K_2(1820)$ | 1.816 | 10 | 0 | 1 | 1/2 | 2.41 | 1 |
| \bar{K}_0^* | 1.425 | 2 | 0 | -1 | 1/2 | 0.93 | 0 | $\bar{K}_2(1820)$ | 1.816 | 10 | 0 | -1 | 1/2 | 2.41 | 0 |
| K_2^* | 1.430 | 10 | 0 | 1 | 1/2 | 1.65 | 1 | $\Lambda(1820)$ | 1.820 | 6 | 1 | -1 | 0 | 0.69 | 0.89* |
| \bar{K}_2^* | 1.430 | 10 | 0 | -1 | 1/2 | 1.65 | 0 | $\Xi(1820)$ | 1.823 | 8 | 1 | -2 | 1/2 | 0 | 1* |
| $N(1440)$ | 1.440 | 4 | 1 | 0 | 1/2 | 1.4 | 0 | $\Lambda(1830)$ | 1.830 | 6 | 1 | -1 | 0 | 1.31 | 0.45* |
| $\rho(1450)$ | 1.465 | 9 | 0 | 0 | 1 | 2 | 0 | $\phi_3(1850)$ | 1.854 | 7 | 0 | 0 | 0 | 0.5 | 0.75 |
| $a_0(1450)$ | 1.472 | 3 | 0 | 0 | 1 | 2.38 | 0.33 | $\pi_2(1880)$ | 1.895 | 15 | 0 | 0 | 1 | 4.85 | 0 |
| $\eta(1475)$ | 1.476 | 1 | 0 | 0 | 0 | 1 | 1 | $\Lambda(1890)$ | 1.890 | 4 | 1 | -1 | 0 | 0.87 | 0.62* |
| $f_0(1500)$ | 1.505 | 1 | 0 | 0 | 0 | 2.98 | 0.09 | $\Delta(1905)$ | 1.890 | 24 | 1 | 0 | 3/2 | 1.9 | 0 |
| $\Lambda(1520)$ | 1.520 | 4 | 1 | -1 | 0 | 0.62 | 0.45* | $\Delta(1910)$ | 1.910 | 8 | 1 | 0 | 3/2 | 1.78 | 0 |
| $N(1520)$ | 1.520 | 8 | 1 | 0 | 1/2 | 1.4 | 0 | $\Delta(1920)$ | 1.920 | 16 | 1 | 0 | 3/2 | 1.88 | 0 |
| $f_2'(1525)$ | 1.525 | 5 | 0 | 0 | 0 | 0.42 | 0.89 | $\Delta(1930)$ | 1.930 | 24 | 1 | 0 | 3/2 | 1.9 | 0 |
| $\Xi(1530)$ | 1.533 | 8 | 1 | -2 | 1/2 | 1 | 0 | $\Delta(1950)$ | 1.930 | 32 | 1 | 0 | 3/2 | 1.8 | 0 |

^a Values with asterisk correspond to antihyperons.

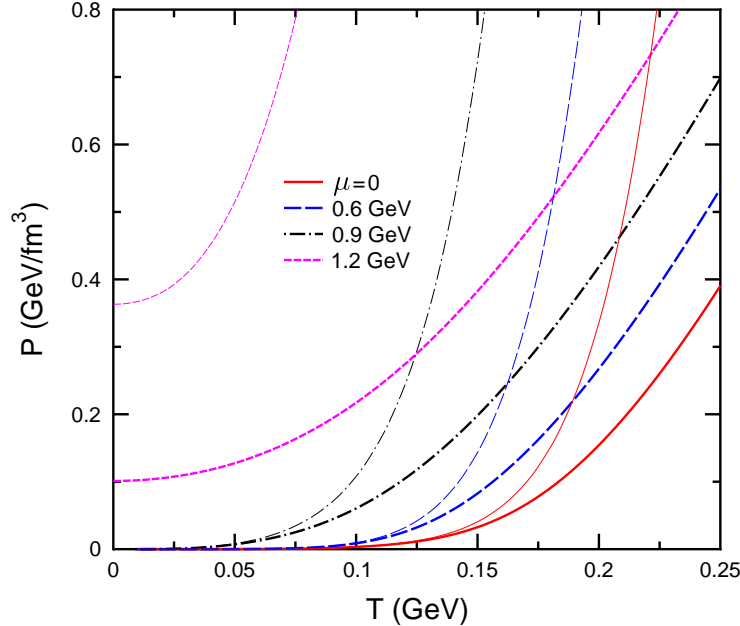


FIG. 1: Pressure of nonstrange hadronic system as a function of temperature at different values of the baryon chemical potential μ . Thick and thin lines correspond to the excluded volume values $v = 1 \text{ fm}^3$ and $v = 0$, respectively.

and μ . At $\mu \gtrsim 1 \text{ GeV}$ it is large for any T . Pressure isotherms as functions of μ are shown in Fig. 2. In accordance with Eq. (10), smaller derivatives of the isotherms imply lower baryon densities at $v \neq 0$ as compared with the case $v = 0$. This is indeed seen in Fig. 3. As expected, the saturating behavior $n \rightarrow 1/v$ is predicted at $\mu \rightarrow \infty$.

To demonstrate sensitivity of the hadronic EOS to the strange chemical potential μ_S , in Fig. 4 we compare isotherms of pressure calculated assuming either $n_S = 0$ or $\mu_S = 0$ (in the latter case the strangeness neutrality is not guaranteed). One can see that deviations caused by nonzero μ_S increase with μ , but they are rather small, especially at low T . Comparison of μ_S -isotherms as functions of μ , calculated with and without EVC, is shown in Fig. 5. For $v \neq 0$ the model predicts almost linear relation between μ_S and μ with the slope of about $1/2$. The deviations from the ideal gas of point-like hadrons ($v = 0$) become important at $\mu \gtrsim 1 \text{ GeV}$.

In connection with nonzero μ_S one has to study the possibility of the K -meson condensation in a dense hadronic medium. This problem is under investigation for more than two decades [23]. As well known, the Bose condensation of the i -th mesonic species

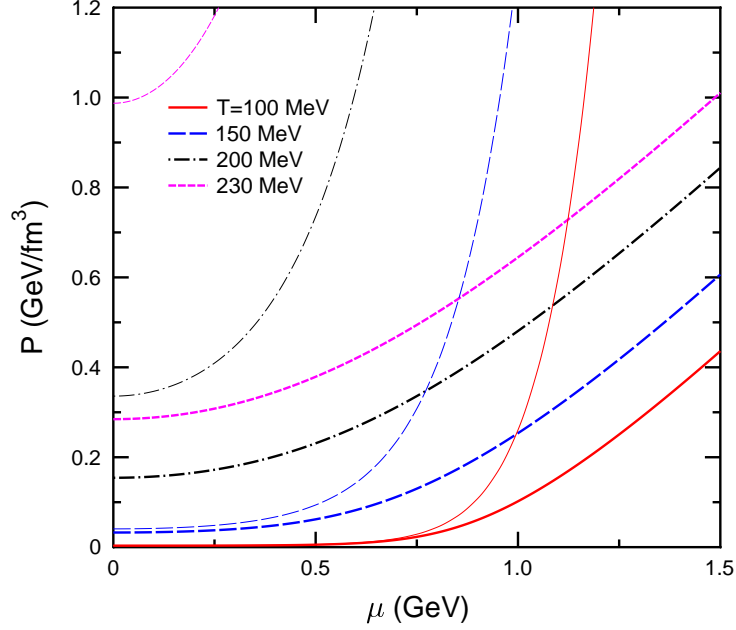


FIG. 2: Pressure isotherms for nonstrange hadronic system as functions of the baryon chemical potential μ . Thick and thin lines correspond to values $v = 1 \text{ fm}^3$ and $v = 0$, respectively.

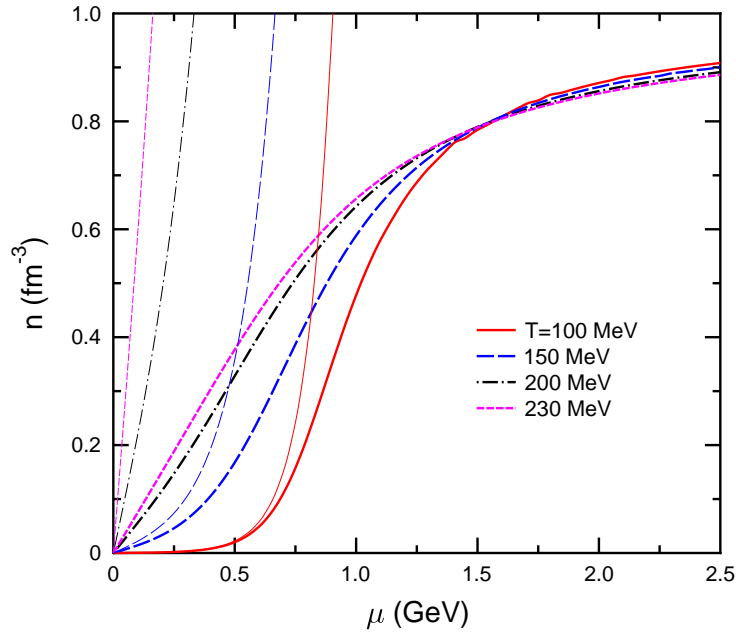


FIG. 3: Same as Fig. 2 but for isotherms of baryon density.

becomes possible if the effective chemical potential (4) exceeds the meson mass m_i [60]. Within the considered model one may expect positive chemical potentials $\tilde{\mu}_i$ only for

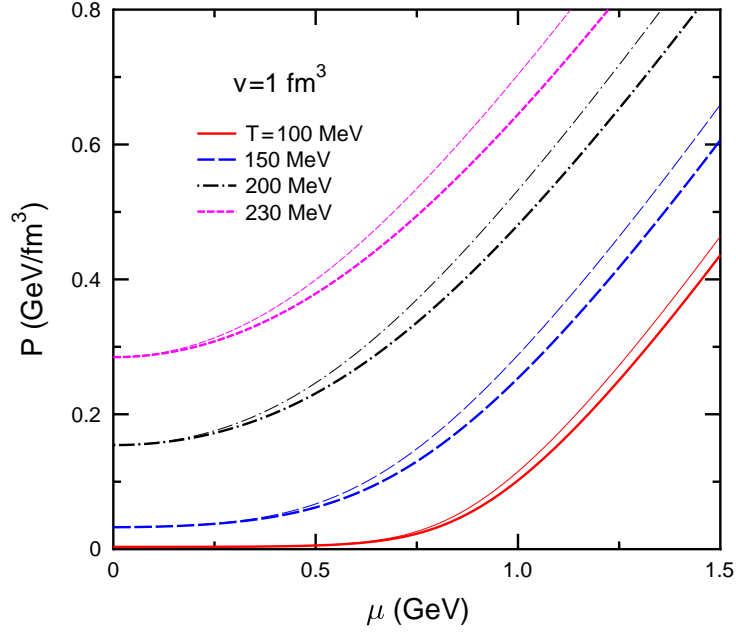


FIG. 4: Pressure isotherms of hadronic system. Thick and thin lines are calculated assuming $n_S = 0$ and $\mu_S = 0$, respectively. All curves correspond to $v = 1 \text{ fm}^3$.

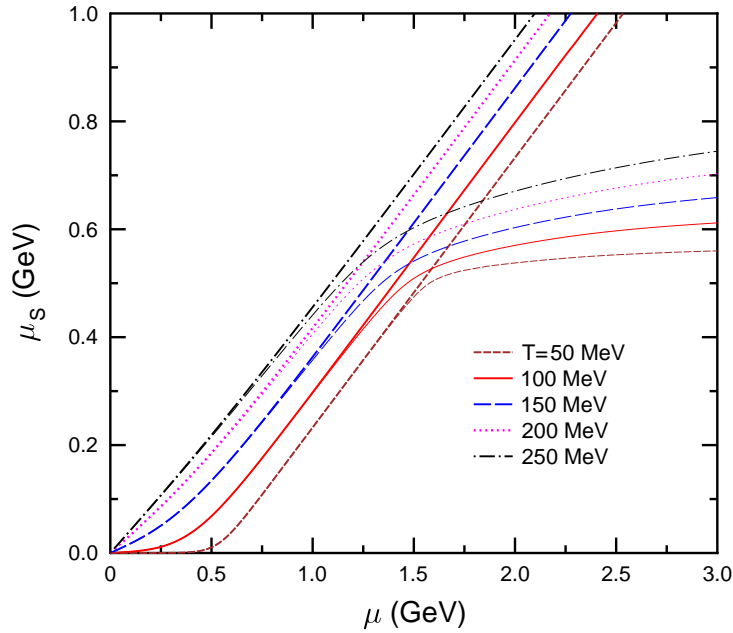


FIG. 5: Isotherms of μ_S for nonstrange hadronic system: thin and thick lines correspond to $v = 0$ and $v = 1 \text{ fm}^3$, respectively.

strange mesons with $S_i = 1$. In this respect the most "dangerous" are K^+ mesons with

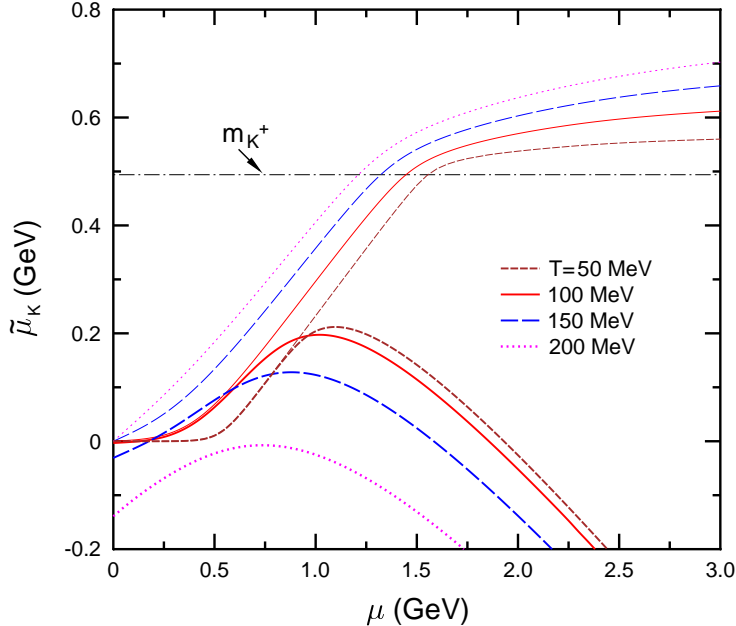


FIG. 6: The effective chemical potential of kaons as a function of μ at different temperatures T . Thin and thick lines are calculated assuming $v = 0$ and $v = 1 \text{ fm}^3$, respectively. The dashed-dotted line shows the threshold of the K^+ -meson condensation.

mass $m_{K^+} \simeq 494 \text{ MeV}$. As one can see from Fig. 6, in the case $v = 0$ the Bose-condensation of K^+ mesons would be possible at $\mu \gtrsim 1 \text{ GeV}$. However, in the calculation with high enough v , the effective chemical potential $\tilde{\mu}_K$ does not exceed the condensation threshold at any μ and T . Thus, the EVC result in total suppression of the K^+ -condensation in chemically equilibrated hadronic matter with $n_S = 0$. It would be interesting to repeat this analysis for nonzero n_S expected in stellar environments.

C. Hadron multiplicity ratios in heavy-ion collisions

In this section we discuss an interesting behavior of the K^+/π^+ and Λ/π^- multiplicity ratios observed in relativistic heavy-ion collisions by the NA49 Collaboration [7, 8]. The experimental data show a peak ("horn") at low SPS energies. Our consideration follows closely the thermal model used in Refs. [27, 28]. It is assumed that production of secondary hadrons in a nuclear collision can be described as the emission from a statistically equilibrated volume of hadronic matter characterized by certain temperature and baryon chemical potential. Within this model the kaon to pion multiplicity ratio equals n_K^*/n_π^*

TABLE II: Temperature and chemical potentials obtained by thermal fit of hadron ratios in central Au+Au and Pb+Pb collisions at different c.m. bombarding energies $\sqrt{s_{NN}}$.

| $\sqrt{s_{NN}}$, GeV | T , MeV | μ , MeV | μ_S , MeV |
|-----------------------|-----------|-------------|---------------|
| 2.70 | 67 | 735 | 122.5 |
| 3.32 | 85 | 668 | 115.7 |
| 3.84 | 97 | 621 | 111.7 |
| 4.30 | 106 | 584 | 108.5 |
| 4.85 | 117 | 545 | 107.6 |
| 6.41 | 132 | 460 | 94.9 |
| 7.74 | 141 | 405 | 86.4 |
| 8.87 | 147 | 368 | 80.9 |
| 12.4 | 155 | 287 | 64.0 |
| 17.3 | 159 | 219 | 48.5 |
| 62.4 | 164 | 69 | 15.1 |
| 130 | 164 | 34 | 7.4 |
| 200 | 164 | 22 | 4.8 |
| 5500 | 164 | 0.8 | 0.2 |

where n_K^* and n_π^* are, respectively, the equilibrium densities of kaons and pions including those produced in decays of hadronic resonances. We apply the following relations

$$n_\pi^* = \sum_i d_i^\pi n_i, \quad n_K^* = \sum_i d_i^K n_i. \quad (17)$$

Here $n_i = n_i(\mu, \mu_S, T)$ is the partial density of i -th hadrons at fixed μ, μ_S and T calculated by Eq. (13). As before, μ_S is determined from the condition of strangeness neutrality (8). The numerical values of d_i^π and d_i^K are listed in Table I. By definition, these factors equal unity for directly produced pions and kaons, and they are zero for stable hadrons with $i \neq \pi, K$. In our calculations we use the chemical freeze-out parameters μ, T determined from thermal fits of hadronic ratios measured at the AGS, SPS and RHIC energies. Namely, we apply the parametrizations of μ, T as functions of the bombarding energy $\sqrt{s_{NN}}$ given in Ref. [29]. In this way we get the values listed in Table II. The last column of the table gives $\mu_S = \mu_S(\mu, T)$ calculated by using Eqs. (3)–(5), (8)–(11) for the case $v = 1 \text{ fm}^3$. The last line is obtained by extrapolating the parametrizations of μ, T to the LHC energy.

In Fig. 7 we show the densities n_π^*, n_K^* as well as the baryon density (at freeze-out stage), calculated by using the T, μ, μ_S values from Table II. According to this calculation, the max-

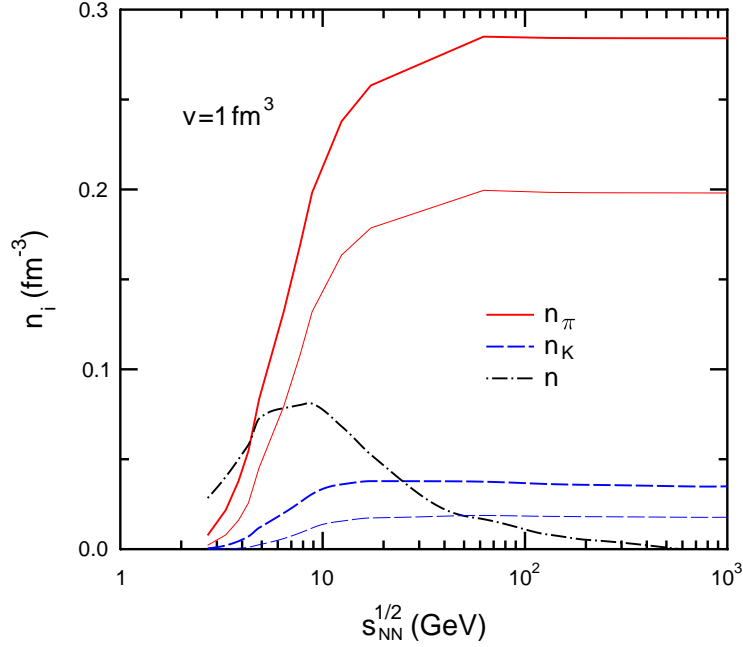


FIG. 7: Total densities of pions (thick solid line) and kaons (thick dashed line) at chemical freeze-out in central heavy-ion collisions as functions of c.m. bombarding energy ($v = 1 \text{ fm}^3$). Thin lines give the contributions to pion and kaon densities from resonance decays. The dashed-dotted line shows the net baryon density.

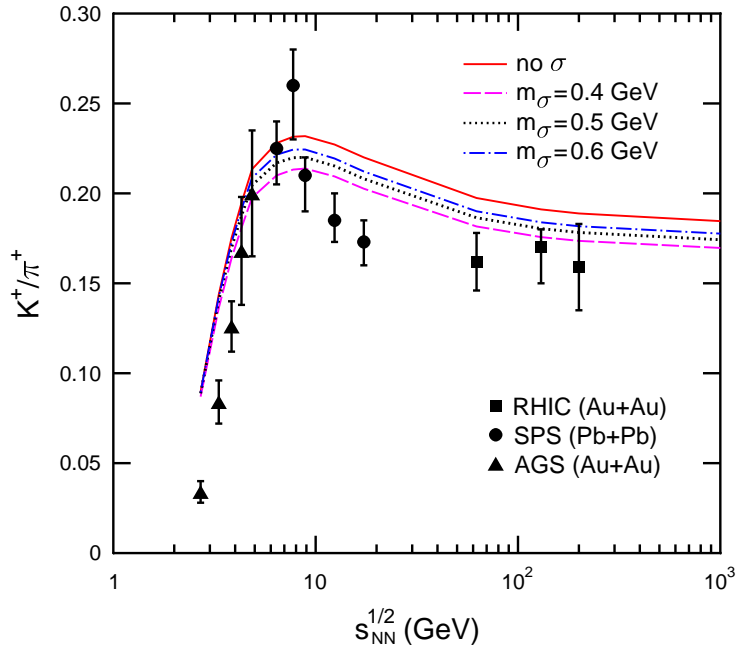


FIG. 8: The K^+/π^+ multiplicity ratio in central nuclear collisions as a function of c.m. bombarding energy ($v = 1 \text{ fm}^3$). Experimental data are taken from Refs. [7, 8, 30, 31].

imal baryon density of about $0.5n_0$ is reached at $\sqrt{s_{NN}} \simeq 9 \text{ GeV}$ ($E_{\text{lab}} = 40 \text{ AGeV}$). One can

see that the pion density saturates at $\sqrt{s_{NN}} \gtrsim 40$ GeV on the level of about 0.3 fm^{-3} . On the other hand, the maximal kaon density $\sim 0.04 \text{ fm}^{-3}$ is reached already at $\sqrt{s_{NN}} \sim 10$ GeV. It is interesting to note that at high energies the contributions of resonance decays reach about 70% and 50% in the case of pions and kaons, respectively.

In Fig. 8 we compare our results for the K^+/π^+ ratio [61] with experimental data obtained at the AGS [30], SPS [7, 8] and RHIC [31] energies. The solid line represents our standard calculation, where the broad $f_0(600)$ resonance (σ meson) is disregarded. One can see that our model is able to reproduce qualitatively the observed K/π ratios but the agreement with data is not perfect. In particular, the experimental data exhibit a much sharper peak at $\sqrt{s_{NN}} \simeq 7.74$ GeV. Choosing different values of v gives only slight modifications and does not improve the shape of the K/π excitation function. This is easy to understand since the EVC are practically cancelled out in hadron multiplicity ratios.

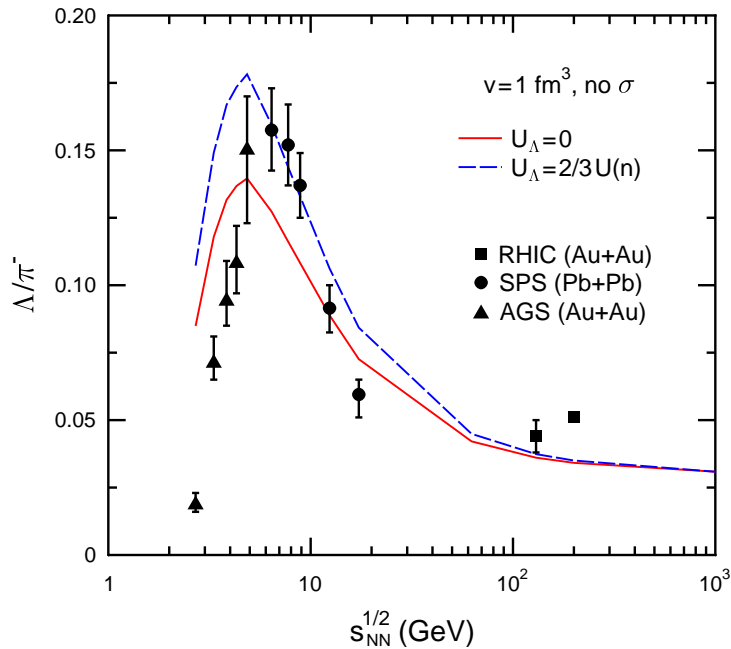


FIG. 9: The Λ/π^- multiplicity ratio in central nuclear collisions as a function of c.m. bombarding energy ($v = 1 \text{ fm}^3$). The dashed lines are calculated with inclusion of additional mean-field potential of Λ hyperons. Experimental data are taken from Refs. [7, 8, 30, 31, 32, 33].

Recently, the authors of Ref. [29] have noticed that these data can be better reproduced by the thermal model which takes into account the contribution of the $f_0(600)$ resonance. To verify this observation, we have made additional calculations including this meson. These calculations are done in the zero-width approximation assuming different masses of σ me-

son, m_σ , and using the values $g_\sigma = 1$, $d_\sigma^\pi = 2$, $d_\sigma^K = 0$. As seen in Fig. 8 visible changes in the K^+/π^+ ratio take place at $\sqrt{s_{NN}} \gtrsim 5$ GeV. However, even at smallest $m_\sigma \simeq 0.4$ GeV, due to increased pion multiplicity, this ratio drops only by about 10%. At the same time, the observed values in the peak region are underestimated stronger in this case. As expected, the shifts of the K^+/π^+ ratio become smaller for larger m_σ . On the basis of this analysis, we conclude that the inclusion of the σ meson does not solve the problem. According to Ref. [34], to obtain a better fit of data one should introduce an additional parameter $\gamma_S < 1$ which is responsible for the suppression of strange hadron yields compared to the equilibrium model predictions.

We have also calculated the excitation function of the Λ/π^- ratio. The results are shown in Fig. 9. One can see that the model can qualitatively reproduce the experimental data, although the peak height is somewhat underestimated. Our analysis shows that the agreement with the data can be improved if one takes into account an additional mean-field potential of Λ hyperons, $U_\Lambda = \frac{2}{3}U(n)$ [62], where $U(n)$ is the corresponding Skyrme-like potential for nucleons introduced in Sect. V A.

Finally, we would like to emphasize that a nonmonotonous behavior of the K/π and Λ/π excitation functions is obtained without any reference to the QGP. Within our model this anomaly is mainly related to the strangeness neutrality condition which in turn requires nonzero μ_S in the hadronic phase. In the Boltzmann approximation the K/π and Λ/π ratios are approximately proportional to y_K and y_Λ defined as

$$y_K = \exp[(\mu_S - m_K + m_\pi)/T], \quad y_\Lambda = \exp[(\mu - \mu_S - m_\Lambda + m_\pi)/T]. \quad (18)$$

According to our calculations these functions have maxima at $\sqrt{s_{NN}} \simeq 9$ and 5 GeV, respectively. The appearance of these maxima follows from a nonmonotonous behavior of the strangeness fugacity $\exp(\mu_S/T)$ along the chemical freeze-out line [63]. As demonstrated above, this behavior agrees qualitatively with experimental data. The inclusion of resonance decays makes the K/π and Λ/π peaks more pronounced.

III. QUARK–GLUON PHASE WITHIN THE BAG MODEL

To calculate thermodynamic properties of a baryon-rich QGP we use a simple bag model with perturbative corrections of the order α_s . Gluons ($i = g$) and light quarks ($i = q, \bar{q}$)

are considered as massless point-like particles, but for strange quarks ($i = s, \bar{s}$) we introduce a nonzero mass m_s . Nonperturbative effects are introduced via the bag constant B . In the chemically equilibrated QGP, one can again express the chemical potential of the i -th particle by Eq. (5), where μ and μ_S are now the baryon and strange chemical potentials of the quark-gluon system. As a result, we get the relations $\mu_g = 0$, $\mu_q = -\mu_{\bar{q}} = \mu/3$, $\mu_s = -\mu_{\bar{s}} = \mu/3 - \mu_S$.

Following Ref. [35] we take into account perturbative corrections by introducing additional constant factors $1 - \xi$ and $1 - 0.8\xi$ into the kinetic pressure of quarks and gluons, respectively. Here $\xi \sim \alpha_s$ is the model parameter which we fix by the comparison with lattice data. Within such an approach one gets the following expression for pressure of the QGP:

$$P = \left(\tilde{N}_g + \frac{21}{2} \tilde{N}_f \right) \frac{\pi^2 T^4}{90} + \tilde{N}_f \left(\frac{\mu^2 T^2}{18} + \frac{\mu^4}{324 \pi^2} \right) + \frac{1 - \xi}{\pi^2} \int_{m_s}^{\infty} d\epsilon (\epsilon^2 - m_s)^{3/2} \left\{ \frac{1}{e^{\frac{\epsilon - \mu_s}{T}} + 1} + \frac{1}{e^{\frac{\epsilon + \mu_s}{T}} + 1} \right\} - B. \quad (19)$$

Here $\tilde{N}_g = 16(1 - 0.8\xi)$ is the effective number of gluons and $\tilde{N}_f = 2(1 - \xi)$ is the effective number of light flavors. The third term in Eq. (19) gives the contribution of strange quarks and antiquarks. Corresponding expressions for densities of baryon charge n , strangeness n_S , energy ϵ and entropy s can be obtained from Eq. (19) by using the thermodynamic relations (7), (14). One can easily see that the strangeness density of the QGP, $n_S = n_{\bar{s}} - n_s = \partial P / \partial \mu_S$, vanishes if $\mu_s = \mu_S - \mu/3 = 0$.

Below we fix $m_s = 150 \text{ MeV}$ and take the same value $B = 344 \text{ MeV/fm}^3$ as in our previous fluid-dynamical calculations (EOS-I) [36, 37] of heavy-ion collisions at RHIC energies. We have calculated the thermodynamic functions of the QGP for different values of the parameter ξ . Motivated by the comparison with lattice data (see Fig. 11), we further use the value $\xi = 0.2$ in our calculations. The advantage of the bag model is that it can be used in the region of nonzero chemical potential, which is still not accessible by lattice calculations. In Fig. 10 we show pressure isotherms of strange ($\mu_S = 0$) and nonstrange ($\mu_S = \mu/3$) QGP. Similarly to the hadronic matter (see Fig. 4), in the case of nonzero μ_S the pressure is reduced compared to the calculation with $\mu_S = 0$.

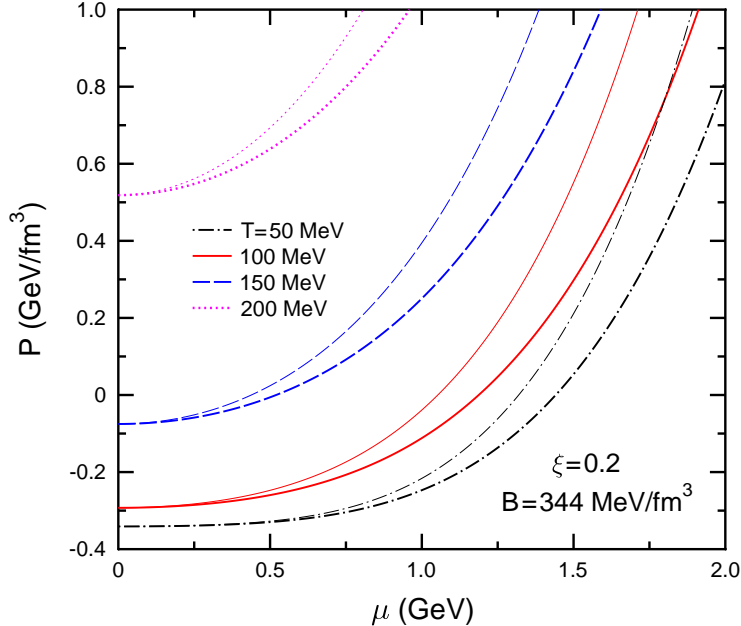


FIG. 10: Same as Fig. 4, but for pressure isotherms of the quark–gluon plasma. Notice the appearance of negative pressure values at low T and μ .

IV. THE DECONFINEMENT PHASE TRANSITION AND PROPERTIES OF MIXED PHASE

A. Phase equilibrium conditions

Below we use our phenomenological approach, where the hadronic and quark–gluon phases are described by two different models, to study the possibility of a first order deconfinement phase transition. If such a transition exists, then only three types of equilibrium states are possible at a given point in the (μ, μ_S, T) space: the hadronic phase (HP), the quark–gluon phase (QP) and the mixed phase (MP). Outside the MP region the stable phase is the one which has a higher pressure [12]. The Gibbs condition of equilibrium between the domains of different phases in the MP can be written as

$$P_H(\mu, \mu_S, T) = P_Q(\mu, \mu_S, T). \quad (20)$$

Here and below we mark thermodynamic functions of the hadronic and quark–gluon phases by indices H and Q , respectively. The expressions for pressure P_H and P_Q are given in Sect. II A and III.

In a baryon–rich mixed phase the condition of zero total strangeness leads to the

strangeness–antistrangeness separation phenomenon [20]. At nonzero μ and T , the equations $n_{SH} = n_{SQ} = 0$ may hold simultaneously with Eq. (20) only in a single point of the (μ, μ_S, T) space. But in general, the strangeness numbers of coexisting domains are nonzero and compensate each other only on average over the total volume of the system. Let λ denotes the volume fraction of hadronic domains in the MP:

$$\lambda = \frac{V_H}{V_H + V_Q} \in [0; 1], \quad (21)$$

where V_H and V_Q are the total spatial volumes occupied by hadrons and the QGP, respectively. Then the condition of zero total strangeness may be written as

$$n_S = \lambda n_{SH} + (1 - \lambda) n_{SQ} = 0. \quad (22)$$

This condition holds if n_{SH} and n_{SQ} have different signs. At fixed μ, λ the phase transition temperature T_c is determined by solving Eqs. (20), (22). The phase transition region in the $\mu - T$ plane is not a line, but a strip [21] $T = T_c(\mu, \lambda)$ where T_c is decreasing function of λ . The lines $T = T_c(\mu, 1)$ and $T = T_c(\mu, 0)$ give the hadronic and quark–gluon boundaries of the MP. Our calculations show (see Fig. 15) that the strip’s width decreases with increasing excluded volume v .

The energy, baryon and entropy densities in the MP are calculated by using the first equality of (22) with the replacement of n_S by ϵ, n and s , respectively. At given μ, T we use the values of μ_S, λ obtained by solving Eqs. (20), (22).

B. Results for baryon-free matter

In this section we present our results for the baryon–free system ($\mu = \mu_S = 0$), which can be compared with lattice calculations. Table III gives critical temperatures T_c obtained for different values of ξ . In Fig. 11 we compare the model predictions for ϵ/T^4 with the

TABLE III: Critical temperature of the deconfinement phase transition in the baryon–free matter ($v = 1 \text{ fm}^3, B = 344 \text{ MeV}/\text{fm}^3$).

| ξ | 0 | 0.1 | 0.2 | 0.3 |
|--------------------|-------|-------|-------|-------|
| $T_c, \text{ MeV}$ | 155.4 | 159.9 | 165.1 | 171.3 |

lattice calculations from Ref. [1]. One can clearly see a pronounced peak just above T_c

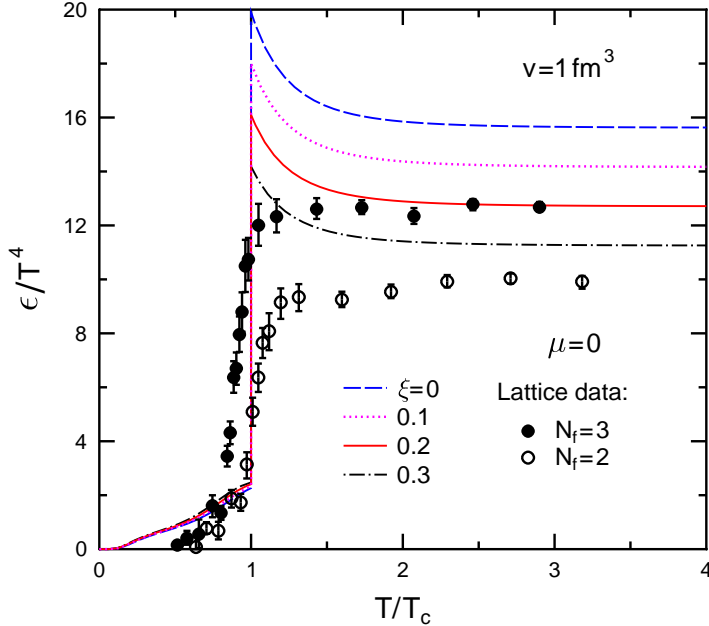


FIG. 11: Scaled energy density of baryon-free matter as a function of scaled temperature at different values of ξ . All results are obtained with $v = 1 \text{ fm}^3$ and $B = 344 \text{ MeV}/\text{fm}^3$. T_c is the critical temperature of the deconfinement phase transition (see Table III). Open and closed circles show the lattice data [1] with the number of quark flavors $N_f = 2$ and 3 , respectively.

which is not present in the lattice data. This is a well-known artefact of the bag model (see e.g. [37]). At high temperatures a good agreement with the lattice data can be achieved by choosing $\xi \simeq 0.2$. Based on these results, we use $\xi = 0.2$ in the following calculations.

A more detailed information about the EOS of baryon-free systems is given in Figs. 12–14. Figure 12 represents the graphic solutions of Eq. (20) for zero and nonzero v . In the case $v = 1 \text{ fm}^3$ the curves $P_H(T)$ and $P_Q(T)$ intersect in a single critical point C . On the other hand, in the calculation with $v = 0$ two crossing points C' and C'' are present. The second point corresponds to the transition QGP \rightarrow HP at the temperature $T = T_{C''} > T_{C'}$. Such unusual behavior, not supported by lattice data, is explained by a too steep rise of pressure of point-like hadrons with increasing number of species at high temperatures.

To perform fluid-dynamical modelling of heavy-ion collisions, one should know pressure as a function of the energy density ϵ and net-baryon density n . Such a representation of the EOS of the baryon-free matter is shown in Fig. 13. In this figure the deconfinement phase transition shows up as a horizontal line connecting the HP and QP. This line corresponds to the MP states. The parameters of the phase transition, calculated for $v = 1 \text{ fm}^3$, are close to

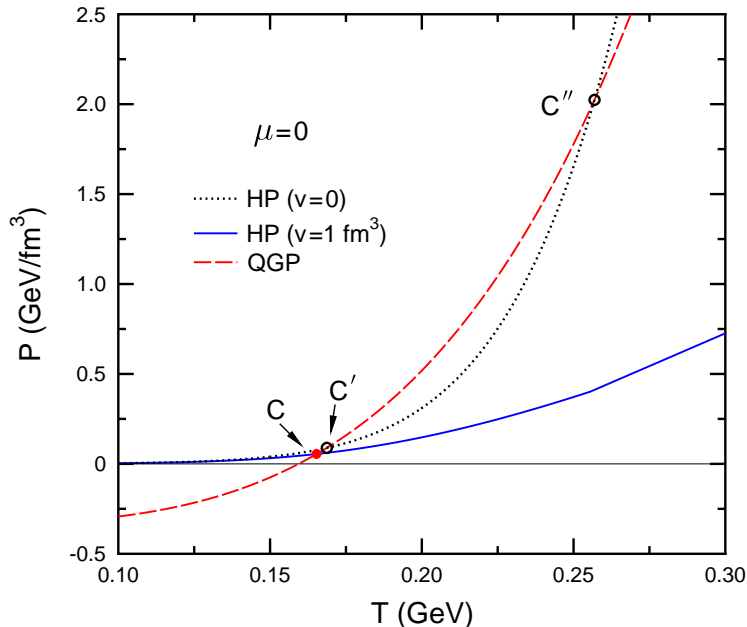


FIG. 12: Pressure of baryon-free matter as a function of temperature. The solid and dotted lines show pressure of the HP calculated with $v = 1 \text{ fm}^3$ and $v = 0$, respectively. The dashed line shows pressure of the QGP calculated with $B = 344 \text{ MeV/fm}^3$ and $\xi = 0.2$.

those in the equation of state EOS-I used in Refs. [36, 37]. The dashed line shows metastable states of the HP extended into the region of large ϵ . At such energy densities, a much harder EOS of the HP is predicted compared to the calculation with $v = 0$ (shown by the dotted line). On the other hand, both calculations give similar results at low ϵ . In fluid-dynamical simulations of heavy-ion collisions [36, 37, 38] two scenarios, with and without the phase transitions, are often compared to check the sensitivity of observables to the EOS. However, from comparing the dashed and dotted lines in Fig. 13, it is evident that such analysis could be misleading if the role of repulsion in a dense hadronic system is ignored.

The sound velocity c_s is an important characteristic of the EOS which gives the speed of small perturbations of matter in its local rest frame. Within the ideal hydrodynamics the sound velocity squared is equal to [12]

$$c_s^2 = \left(\frac{\partial P}{\partial \epsilon} \right)_\sigma = \left(\frac{\partial P}{\partial \epsilon} \right)_n + \frac{n}{w} \left(\frac{\partial P}{\partial n} \right)_\epsilon, \quad (23)$$

where $\sigma = s/n$ is the entropy per baryon and $w = \epsilon + P$ is the enthalpy density. In the second equality we have applied the thermodynamic relation ($n_S = 0$):

$$d\sigma = \frac{1}{nT} (d\epsilon - \frac{w}{n} dn). \quad (24)$$

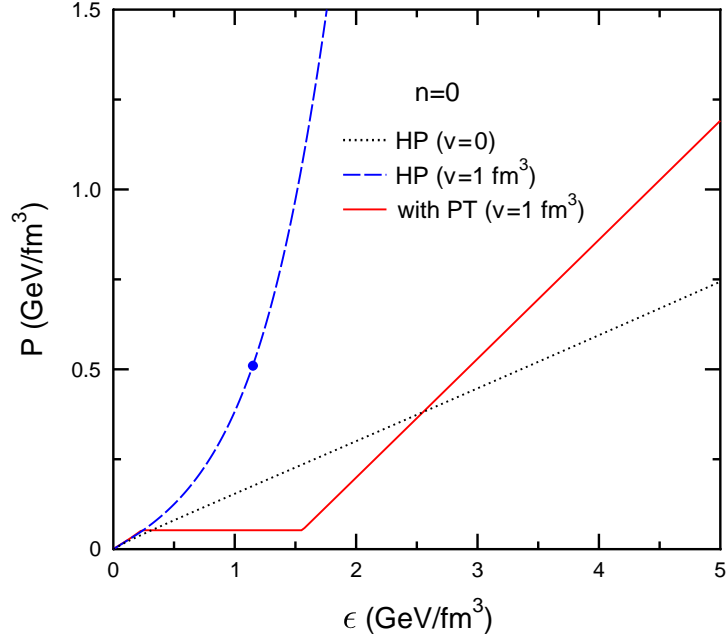


FIG. 13: Pressure of baryon-free matter as a function of energy density. Dashed and dotted lines show pressure of a hadronic system calculated with $v = 1 \text{ fm}^3$ and $v = 0$, respectively. The solid line shows pressure calculated with inclusion of EVC and phase transition effects. Above the dot the HP has superluminal sound velocities.

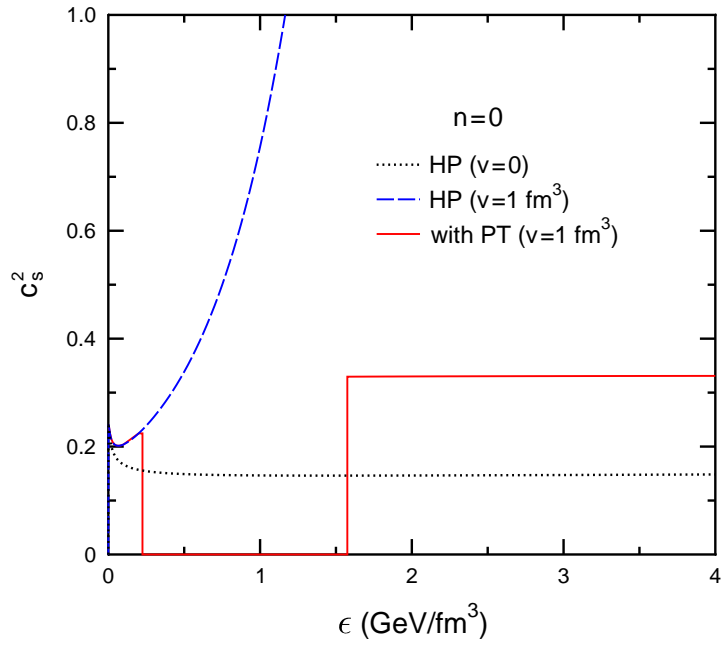


FIG. 14: Same as Fig. 13, but for sound velocity squared.

In the case of baryon-free matter ($n = 0$) c_s^2 is equal to the slope of pressure as a function of ϵ .

The causality condition $c_s < 1$ should be fulfilled in any model consistent with relativistic kinematics. However, a simple Van der Waals approach does not guarantee this property, as has been already mentioned in Refs. [16, 17]. In a gas of hard spheres the acausal behavior is associated with an implicit assumption that the signal propagates instantaneously over the sphere extension. As will be shown below, the causality condition $c_s < 1$ is indeed violated in the HP, but only at rather high baryon densities and small temperatures. For illustration, Fig. 14 shows c_s^2 for baryon-free matter. One can see that c_s^2 is close to $1/3$ in the QP, vanishes in the MP and equals $0.2 - 0.25$ (at $v = 1 \text{ fm}^3$) in the HP. The values $c_s > 1$ are reached only in metastable hadronic states with $\epsilon \gtrsim 1 \text{ GeV}/\text{fm}^3$ which are not realized in the equilibrated matter.

C. Phase diagram in $\mu - T$ plane

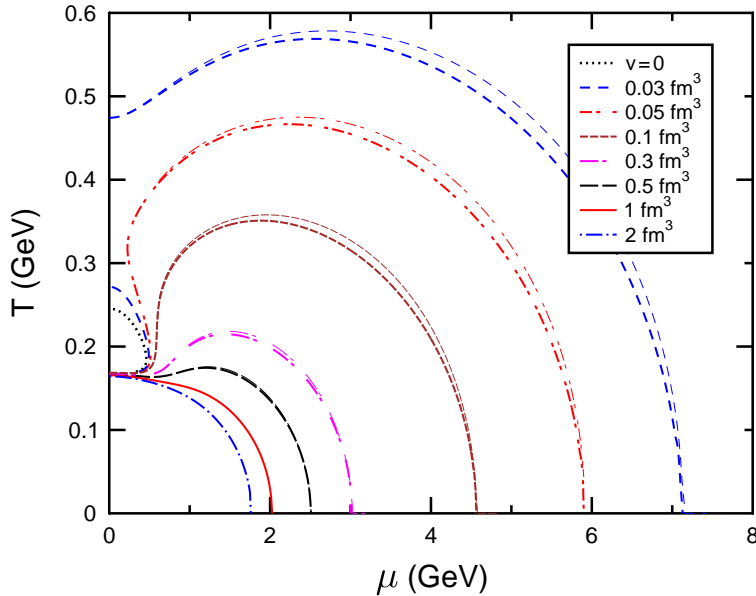


FIG. 15: Phase diagrams in the $\mu - T$ plane calculated for different v . Thick and thin lines correspond to hadronic and quark-gluon boundaries of the MP, respectively.

Using the Gibbs condition (20) we have calculated the phase diagram of matter in the $\mu - T$ plane. The results for different values of v are given in Fig. 15. For each v

we show two boundaries of the MP corresponding to the conditions $n_{SH} = 0$ ($\lambda = 1$) or $n_{SQ} = 0$ ($\lambda = 0$). One can see that the width of the MP region decreases with increasing v . The two boundaries are practically undistinguishable at $v \gtrsim 0.5 \text{ fm}^3$. With decreasing v the HP occupies larger and larger domain of the $\mu - T$ plane. At $v \lesssim 0.1 \text{ fm}^3$ the phase boundary exhibits a back bending at small chemical potentials, $\mu < \mu_* \simeq 0.8 \text{ GeV}$. This means that at fixed $\mu < \mu_*$ and increasing T three phase transitions appear: the first and third ones from the HP to the QGP, and the second intermediate transition, from the QGP to the HP. The third point goes to infinity at $v \rightarrow 0$. This means that the HP is thermodynamically more stable than the QP at asymptotically high temperatures. At $v = 0$ only a small domain of the QGP (its boundary is shown by the dotted line) remains in the $\mu - T$ plane. This is certainly an unphysical behavior, which clearly shows inconsistency of the hadron resonance gas model with point-like hadrons.

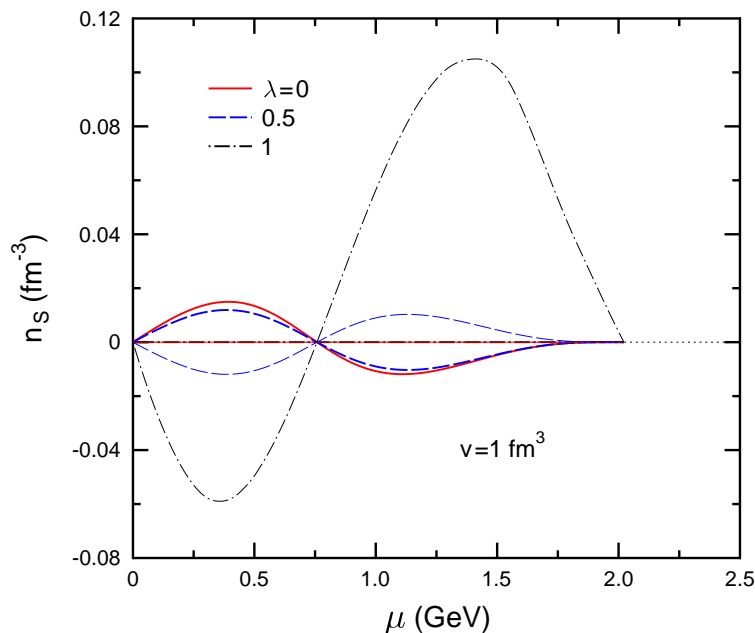


FIG. 16: Strangeness densities of the hadronic (thick lines) and quark–gluon (thin lines) components in the MP region of the phase diagram as functions of the baryon chemical potential. The results are shown for several values of the volume fraction λ . For $\lambda = 0$ (no hadrons) $n_{SQ} = 0$.

Figure 16 shows the strangeness number densities n_{SH} and n_{SQ} across the MP ($v = 1 \text{ fm}^3$). One can see that indeed, n_{SH} and n_{SQ} have different signs (see Sect. IV A), but their absolute values do not exceed 0.1 fm^{-3} . At $\mu \gtrsim 0.8 \text{ GeV}$ (anti)strangeness in hadronic domains is carried mostly by hyperons. According to Fig. 17, at large chemical potentials

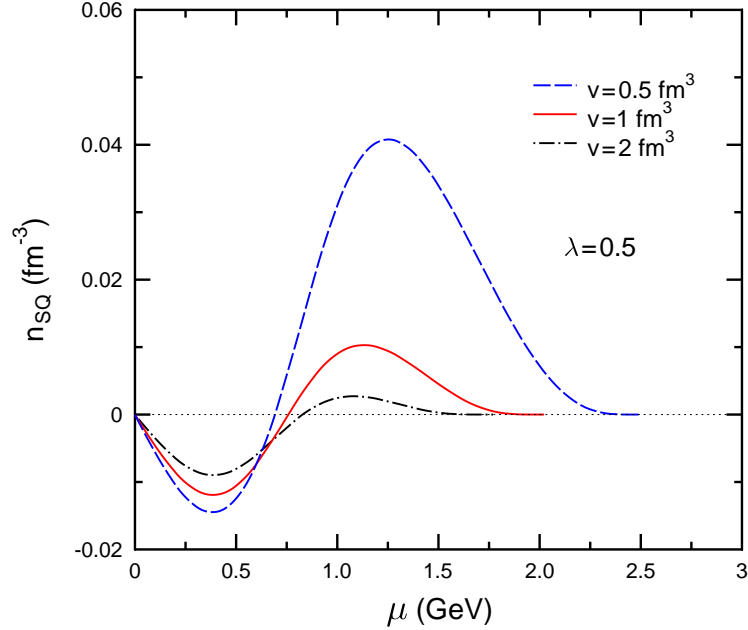


FIG. 17: Strangeness density of the quark–gluon domains in the MP ($\lambda = 0.5$) at different values of the excluded volume v .

the strangeness density n_{SQ} is rather sensitive to v .

D. Adiabatic trajectories

Further on we consider in more details the results for $v = 1 \text{ fm}^3$. In Figs. 18–22 we show the adiabatic trajectories (“adiabates”) i.e. sets of states with equal entropy per baryon, $S/B = \sigma = \text{const}$. As well-known [39], in the ideal hydrodynamics the entropy per baryon is conserved in a given fluid element. Therefore, these trajectories contain an important information about the conditions which can be realized in heavy–ion collisions. Figure 18 shows the phase diagram and corresponding adiabates in the $\mu - T$ plane. In such a representation the adiabates with $S/B = 0$ and $S/B = \infty$ are given, respectively, by the horizontal ($T = 0$) and vertical ($\mu = 0$) axes. Note that at $T \rightarrow 0$ all adiabates with finite μ end in the point $\mu \simeq m_N$, where $m_N = 939 \text{ MeV}$ is the nucleon mass. Moreover, these adiabates have a zigzag-type behavior characteristic for a first order phase transition. This means that along the adiabatic trajectory the temperature grows when the system enters the coexistence region. In other words, the temperature of the HP at $\lambda = 1$ is higher than the temperature of the QP at $\lambda = 0$. Such a picture differs from the predictions of the linear σ model and the Nambu–Jona-Lasinio model [5, 41] for the chiral first order phase transition.

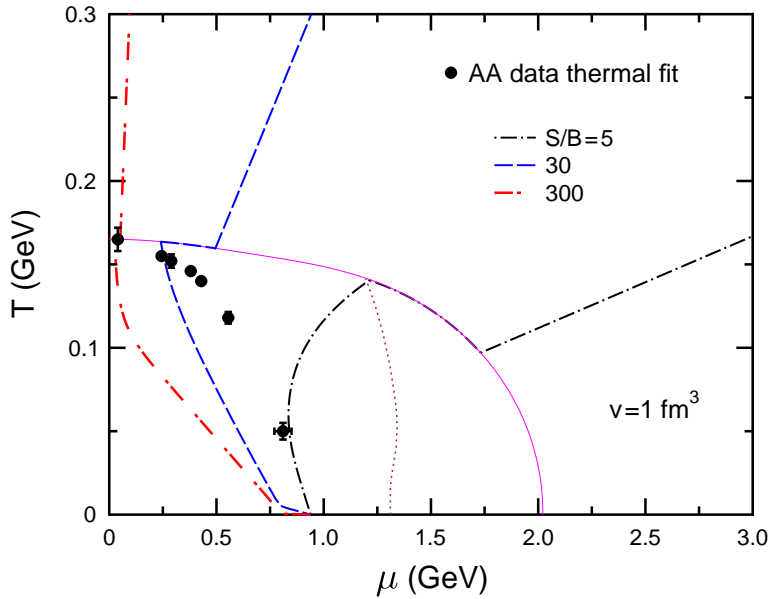


FIG. 18: Lines of constant entropy per baryon in the $\mu - T$ plane ($v = 1 \text{ fm}^3$). The solid curve represents the phase transition line for $\lambda = 0$. Full dots corresponds to the μ, T values obtained from thermal fits of hadron yields [40] observed in central Au+Au and Pb+Pb collisions at different bombarding energies. The region between the dotted and thin solid lines contains states with $c_s > 1$.

There temperature drops in the MP. This difference may be related to the fact that the present model includes massless gluons which are completely ignored in Refs. [5, 41].

Full dots in Fig. 18 show states of the chemical freeze-out [42] in central collisions of heavy nuclei with c.m. bombarding energies from GSI ($\sqrt{s_{NN}} \simeq 2.3 \text{ GeV}$) to RHIC ($\sqrt{s_{NN}} \simeq 200 \text{ GeV}$). "Experimental" values of T and μ have been found [40] from thermal fits of hadron multiplicity ratios observed in such collisions.

A word of caution is in place here. As has been already mentioned, our model contains superluminal sound velocities in the HP. These states are situated in the region between the dotted and thin solid lines in Fig. 18. One can see that such states correspond to values $S/B < 5$. On the other hand, it is known from hydrodynamical simulations (see e.g. [43]) that typical conditions realized in heavy-ion collisions at energies $E_{\text{lab}} \gtrsim 10 \text{ GeV}$ correspond to entropy per baryon $S/B \gtrsim 10$. Therefore, an adiabatically expanding system of particles produced in ultrarelativistic nuclear collisions does not enter the region of $c_s > 1$. However, such states can be reached in compact stars. Based on these results, we conclude

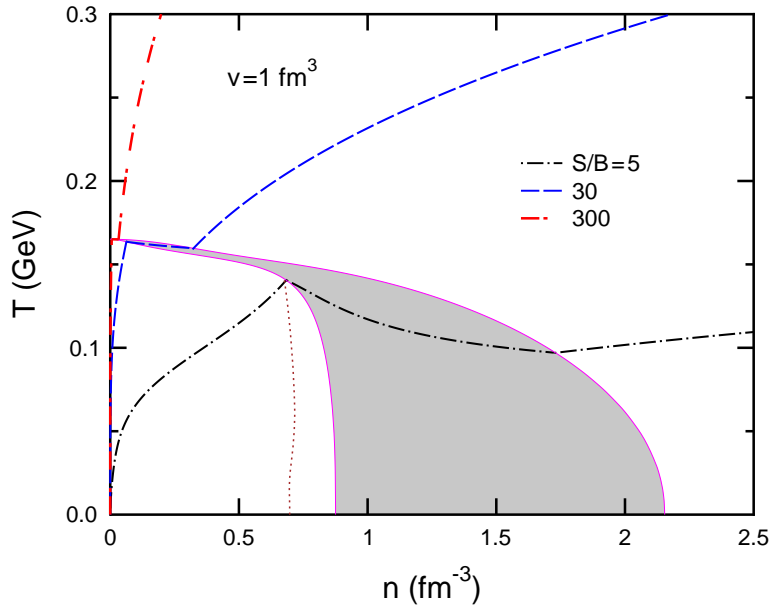


FIG. 19: Boundaries of different phases and adiabatic trajectories in the $n - T$ plane ($v = 1 \text{ fm}^3$). The shaded area shows the mixed phase region. The hadronic states on the right from the dotted line have sound velocities $c_s > 1$.

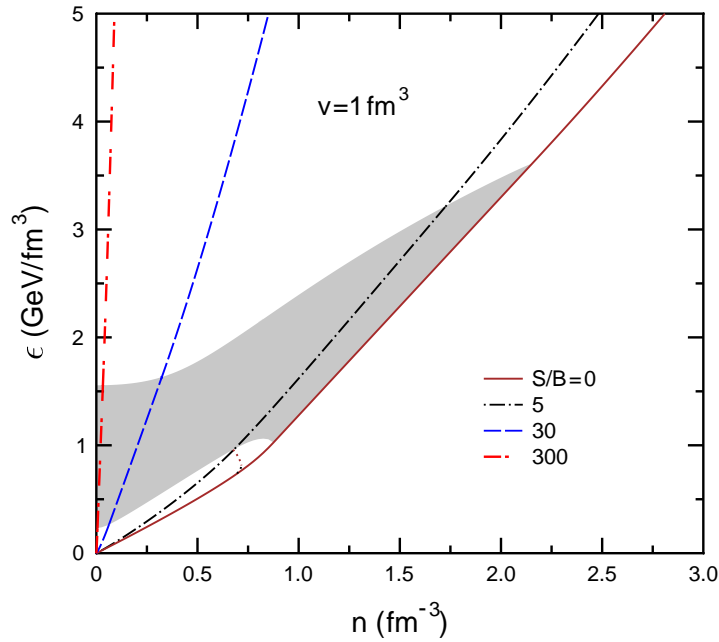


FIG. 20: Same as Fig. 19 but in the $n - \epsilon$ plane.

that the present model should be considerably modified to study properties of the HP and

the deconfinement phase transition at high baryon densities (see the discussion in Ref. [9]).

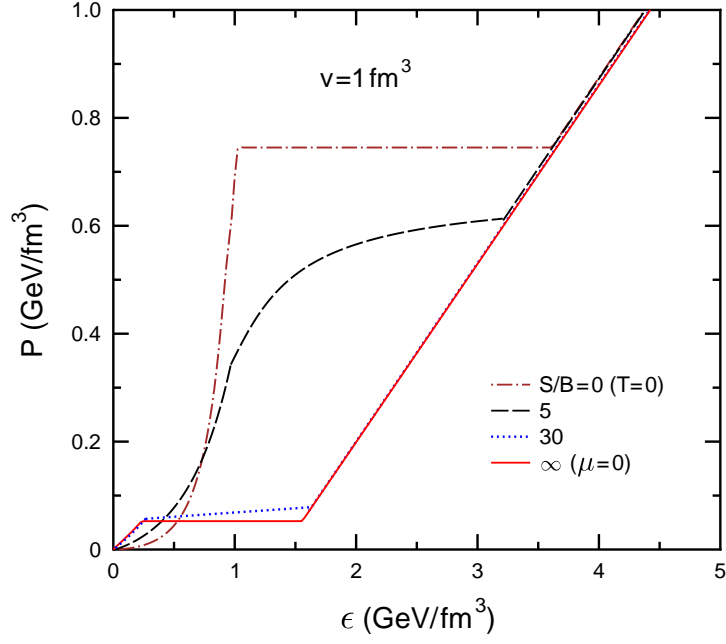


FIG. 21: Adiabatic trajectories in the $\epsilon - P$ plane ($v = 1 \text{ fm}^3$).

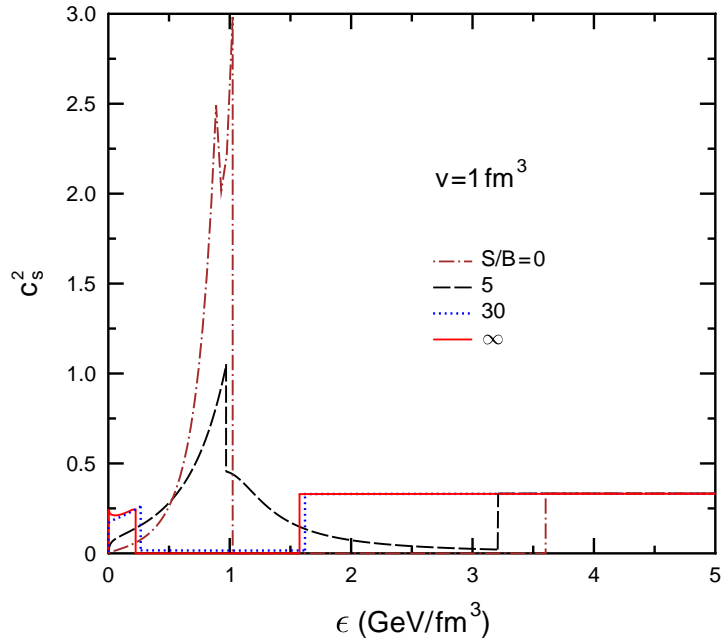


FIG. 22: Sound velocities squared in adiabatic processes with different S/B as functions of energy density ($v = 1 \text{ fm}^3$).

In Figs. 19–20 we show boundaries of different phases in the $n - T$ and $n - \epsilon$ planes.

Again, one can see that adiabates with $S/B \gtrsim 10$ do not enter the "dangerous" region with superluminal sound velocities. The solid line in Fig. 20 corresponds to the limiting case of $T = 0$. States below this line can not exist. Figure 21 shows pressure adiabates versus the energy density. According to first equality of (23), c_s^2 -values are given by slopes of adiabates in this representation. Note, that pressure in the MP is constant along the lines $\mu = \text{const}$ which differ from the lines $\sigma = \text{const}$ in the $n - \epsilon$ plane. The direct calculation of c_s^2 as a function of ϵ gives the results shown in Fig. 22. One can see that c_s^2 values especially large at zero temperature, for states near the MP boundary. Generally, the sound velocities are nonzero in the MP, however, they are much smaller than maximal values of c_s in the HP. The nontrivial two-peak structure of the adiabat with $S/B = 0$ appears due to the contribution of baryonic resonances ($\Delta, N^* \dots$). However, this behavior takes place only in the unphysical region with $c_s > 1$.

V. INTRODUCTION OF THE MEAN-FIELD

A. Skyrme-like parametrization of the mean-field potential

The EOS obtained in preceding sections takes into account only short-range repulsive interactions of hadrons and completely ignores the intermediate-range attractive interaction between baryons. Due to this reason, this EOS does not describe the saturation property of isospin-symmetric nuclear matter at low temperatures. It is well-known that such attractive interaction leads to the liquid-gas (LG) phase transition in nuclear matter at temperatures $T \lesssim 10 \text{ MeV}$ and chemical potentials $\mu \sim \mu_0 = m_N - E_B$, where $E_B \simeq 16 \text{ MeV}$ is the binding energy of cold nuclear matter. This phase transition manifests itself as the multifragmentation phenomenon in intermediate-energy nuclear reactions [44].

To account for the mean-field effects, we introduce an effective potential $U = U(n)$ which depends only on the baryon density n and does not depend on momenta of interacting baryons [64]. Then the baryon's single-particle energy can be obtained simply by adding $U(n)$ to the kinetic energy. In this case the partition function of the hadronic system can be calculated analytically [16]. Again, finite sizes of hadrons are taken into account by the volume reduction (1). As the result, the following formulae for thermodynamic functions of

the HP can be written

$$\mu = \mu_K + U(n), \quad (25)$$

$$P = P_K + P_f(n), \quad (26)$$

$$\epsilon = \epsilon_K + \epsilon_f(n). \quad (27)$$

The "field" contributions (marked by index f) to the energy density and pressure are found as

$$\epsilon_f(n) = nU(n) - P_f(n) = \int_0^n dn_1 U(n_1). \quad (28)$$

The kinetic terms (marked by index K) in Eqs. (25)–(27) are functions of μ_K, μ_S, T calculated by using formulae of Sect. II A with the replacement $\mu \rightarrow \mu_K, P \rightarrow P_K, \epsilon \rightarrow \epsilon_K$. The resulting expressions for P_K and ϵ_K are obtained from Eqs. (3)–(5) and (15), respectively. One can show that the total pressure $P = P(\mu, \mu_S, T)$ satisfies the relation (7). The densities s, n and n_S are given by Eqs. (9)–(11) where now

$$\tilde{\mu}_i = B_i \mu_K + S_i \mu_S - v P_K. \quad (29)$$

In a spirit of the Skyrme approach [45] we parametrize the mean-field potential in the form

$$U(n) = -\alpha \left(\frac{n}{n_0} \right) + \beta \left(\frac{n}{n_0} \right)^\gamma, \quad (30)$$

where n_0 is the saturation density of nuclear matter and α, β, γ are density-independent parameters. In the following we fix γ to a commonly used value 7/6 and choose the remaining parameters from the requirements $P = 0, \epsilon/n = \mu_0 = 923$ MeV at $n = n_0, T = 0$. The values of α, β as well as the incompressibility modulus $K = 9 \partial P / \partial n$ at the saturation point, calculated for different choices of v , are given in Table IV.

TABLE IV: Parameters of the mean-field potential and the incompressibility modulus of equilibrium nuclear matter for different values of the excluded volume.

| v, fm^3 | 0 | 1 | 2 |
|----------------------|-----|-----|-----|
| α, MeV | 352 | 334 | 297 |
| β, MeV | 301 | 277 | 230 |
| K, MeV | 200 | 214 | 264 |

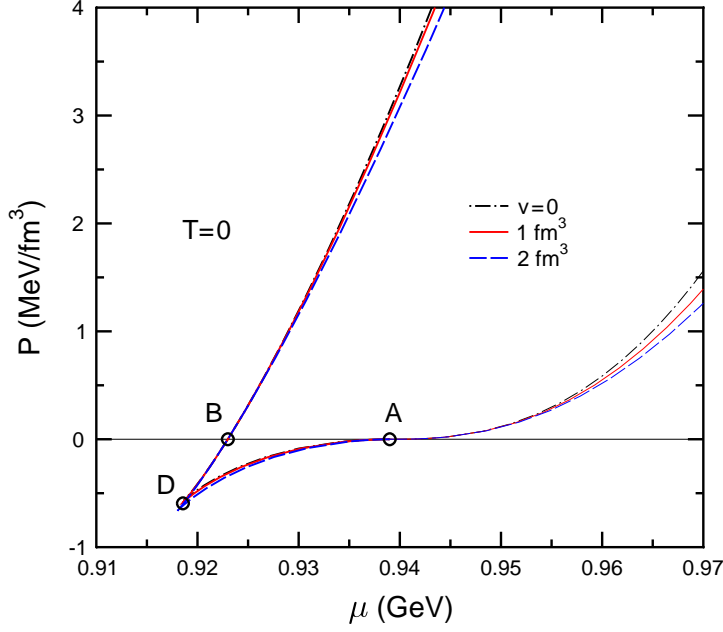


FIG. 23: Pressure of the baryonic system at $T = 0$ as a function of μ for different values of the excluded volume v . Thick and thin lines correspond to the cases $U = U(n)$ and $U = 0$, respectively. The part DA of the thick solid curve represents unstable states for $v = 1 \text{ fm}^3$.

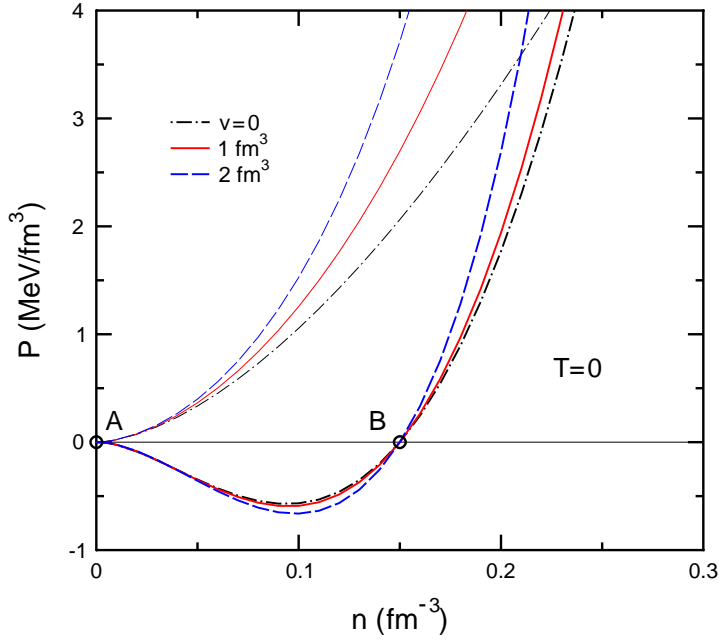


FIG. 24: Same as Fig. 23, but for pressure as a function of the baryon density n .

Figures 23–25 illustrate the properties of cold nuclear matter as predicted by this model. Figure 23 shows pressure as a function of μ for several values of the excluded volume v .

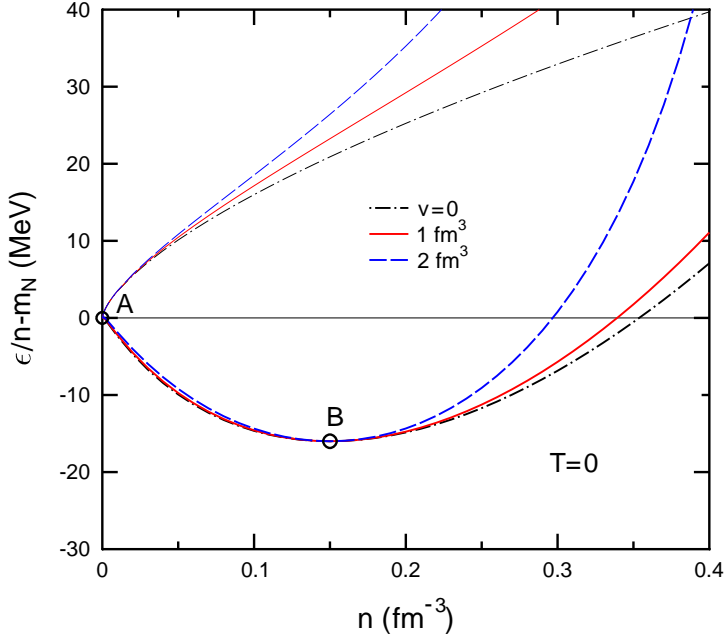


FIG. 25: Same as Fig. 24, but for energy per baryon.

Point B marks the saturation point of cold nuclear matter. The mean-field is responsible for the appearance of several branches of pressure at $\mu < \mu_A = m_N$. In the case $v = 1 \text{ fm}^3$ the branches BA and DB describe the metastable states, while the branch DA corresponds to the unstable states (see below). This behavior differs qualitatively from the case $U = 0$ where only one branch is present at $\mu \geq \mu_A$. Figures 24–25 show pressure and energy per baryon as functions of n . By construction, the saturation point has the same position for all considered values of v .

B. The liquid-gas phase transition

Now let us consider properties of hadronic matter at nonzero temperatures. Figure 26 shows isotherms in the $\mu - P$ plane calculated with $v = 1 \text{ fm}^3$. In this case the existence of the critical point is predicted at the temperature $T_c \simeq 14.925 \text{ MeV}$ and the chemical potential $\mu_c \simeq 909 \text{ MeV}$ (see Table V). The isotherms with $T < T_c$ contain three branches of pressure, similarly to the case $T = 0$ discussed above. The phase transition points correspond to intersections of metastable parts of the isotherms. The branches with negative curvature correspond to unstable (spinodal) states. Small density perturbations will grow exponentially in this region. This is a well-known spinodal instability which leads to the

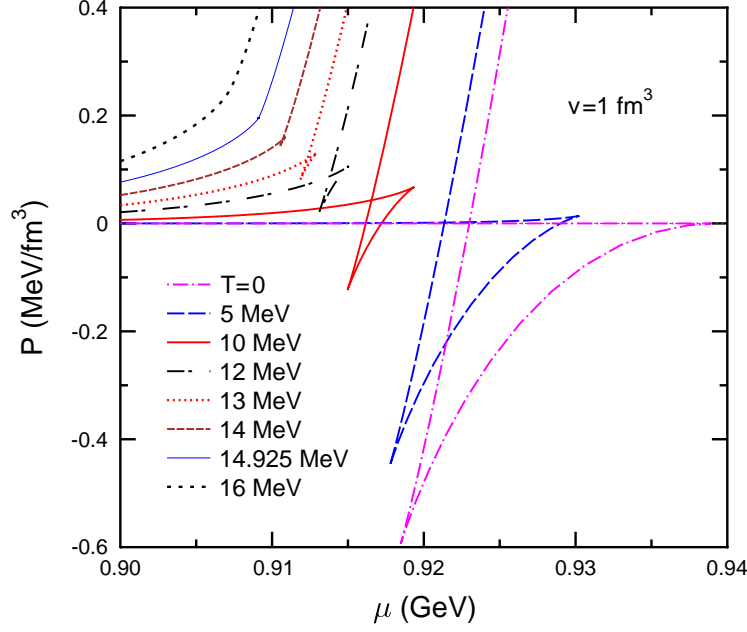


FIG. 26: Isotherms in the $\mu - P$ plane ($v = 1 \text{ fm}^3$).

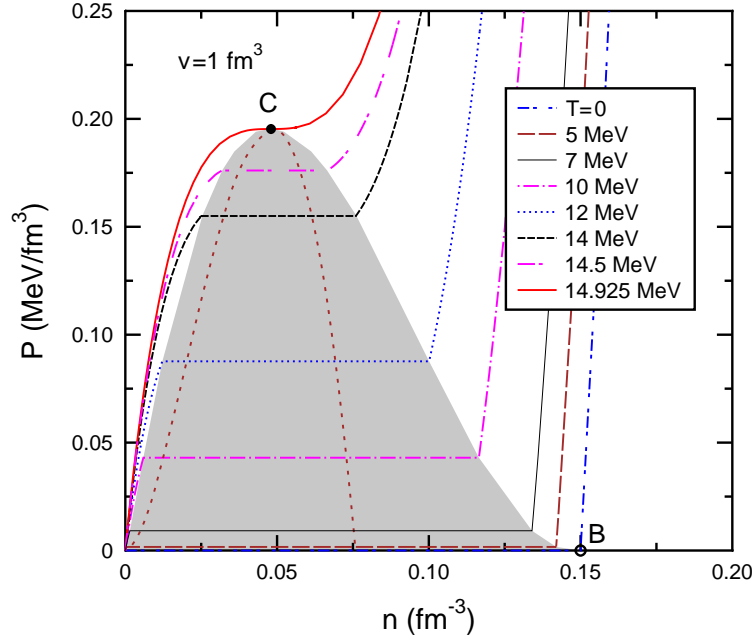


FIG. 27: Pressure isotherms as functions of baryon density ($v = 1 \text{ fm}^3$). The shaded area shows the mixed phase region of the LG phase transition. The dotted line with maximum at point C is the boundary of the spinodal instability domain.

separation of matter into dense and dilute domains [46], characteristic of the LG phase

transition. We would like to note here that the LG mixed phase can be represented by the ensemble of nuclear fragments of different sizes. This ensemble can be well described by the statistical multifragmentation model [47] which also includes the EVC. The anomaly in the caloric curve, associated with the LG phase transition, has been indeed observed in intermediate-energy heavy-ion collisions by the ALADIN collaboration [48].

Figure 27 represents the isotherms in the $n - P$ plane. The shaded region corresponds to the mixed phase, where the hadronic gas (nucleons and light clusters) coexists with nuclear fragments (droplets of liquid). Point C is the critical point of the LG phase transition. The parameters of the critical point for different values of v are given in Table V. One can see

TABLE V: Characteristics of the critical point of the LG phase transition at different values of the excluded volume.

| v, fm^3 | 0 | 1 | 2 |
|-------------------------------|-------|-------|-------|
| T_c, MeV | 15.37 | 14.93 | 12.67 |
| μ_c, MeV | 907 | 909 | 915 |
| n_c, fm^{-3} | 0.048 | 0.048 | 0.039 |
| $P_c, \text{MeV}/\text{fm}^3$ | 0.198 | 0.195 | 0.139 |

that their sensitivity to the excluded volume v is rather weak. This is also seen in Fig. 28 where we compare spinodals and the phase transition lines for $v = 0$ and $v = 1 \text{ fm}^3$. On the basis of these results we conclude that characteristics of the LG phase transition in our model are similar to predictions of other authors (see e.g. [49]).

C. Phase diagram with two phase transitions

Finally we present results for the full model where both the LG and deconfinement phase transitions are included. In the case $T = 0$, applying Eqs. (25)–(30) for a broad interval of baryon densities we get the results shown in Fig. 29. According to our calculations, in the region of the deconfinement phase transition the corrections due to the mean-field interaction are rather small, of the order of 5%. Note that the mean-field potential leads to vanishing pressure for zero temperature states with $n < n_0$ (see Fig. 27).

Figures 30–31, represent the full phase diagram in the $\mu - T$ and $n - T$ planes for $v = 1 \text{ fm}^3$. Compared to the calculation with $U = 0$, a new phase transition line starting at $\mu = \mu_0$ appears in Fig. 30. As seen in Fig. 31, the LG mixed phase (shown by shading) occupies a

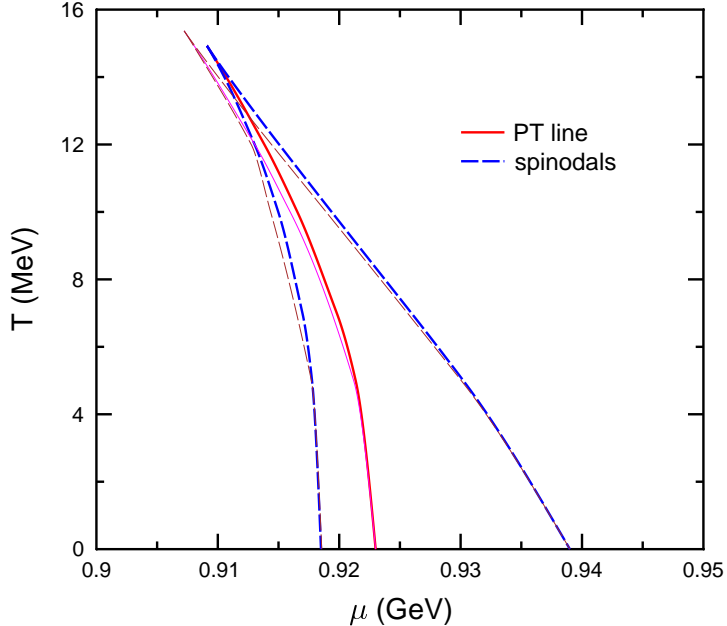


FIG. 28: Phase diagram of the LG phase transition in the $\mu - T$ plane (the solid line). The dashed lines show boundaries of the spinodal region. Thin and thick lines correspond to $v = 0$ and $v = 1 \text{ fm}^3$, respectively.

relatively small region of the $n - T$ plane. According to Fig. 31 the borders of the quark-hadronic mixed phase are shifted only slightly due to the mean-field effects. The same conclusion is valid for the mixed phase boundaries and the $T = 0$ line in the $n - \epsilon$ plane (cf. Fig. 20).

VI. SUMMARY AND DISCUSSION

In this paper we have investigated the EOS of strongly interacting matter in a phenomenological model taking into account the excluded volume effects in the hadronic phase. The quark-gluon phase is described by the bag model with the lowest order perturbative corrections in kinetic terms. Within this approach one can get only a first order phase transition. The sensitivity of the phase diagram to the excluded volume v has been investigated in details. At small values of v the phase diagram has unphysical behavior since the hadronic phase becomes preferable at high temperatures. Only at $v \gtrsim 1 \text{ fm}^3$ the critical temperature of the deconfinement phase transition monotonously decreases with baryon chemical potential μ . Generally, the strength of the phase transition increases with increas-

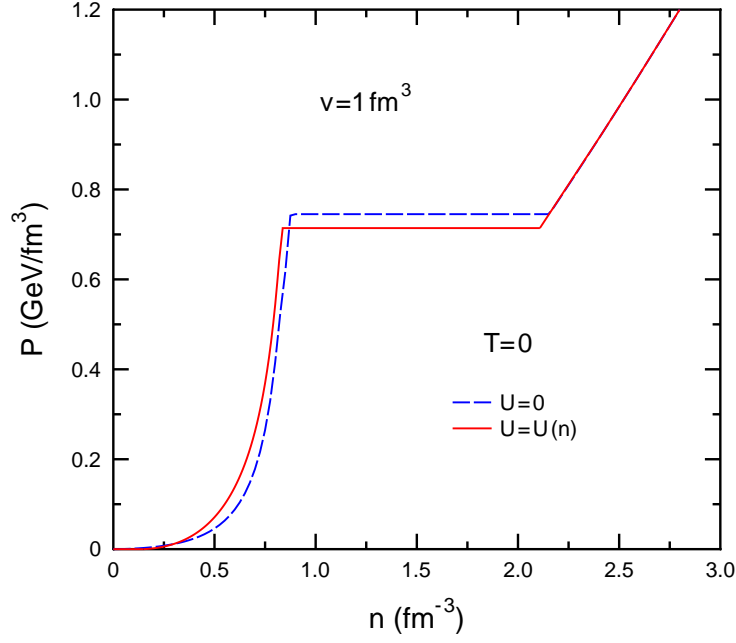


FIG. 29: Pressure as a function of baryon density at $T = 0$. The dashed and solid lines are calculated with and without the mean-field effects, respectively ($v = 1 \text{ fm}^3$). Note change of the vertical scale compared to Figs. 24, 27.

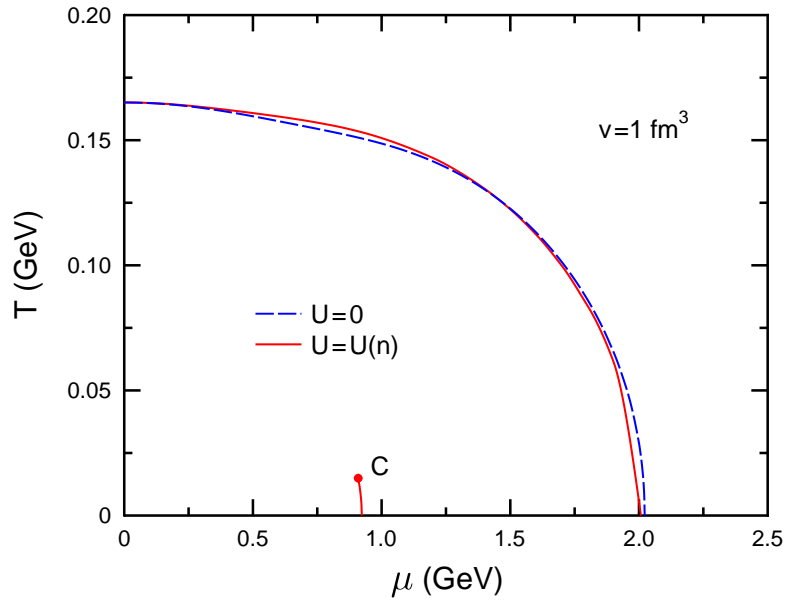


FIG. 30: Phase diagram of strongly interacting matter in the $\mu - T$ plane ($v = 1 \text{ fm}^3$). The dashed and solid lines are obtained from calculations with and without the mean-field effects, respectively.

ing μ . Typical values of the baryon density in the mixed phase are in the range $(5 - 10) n_0$

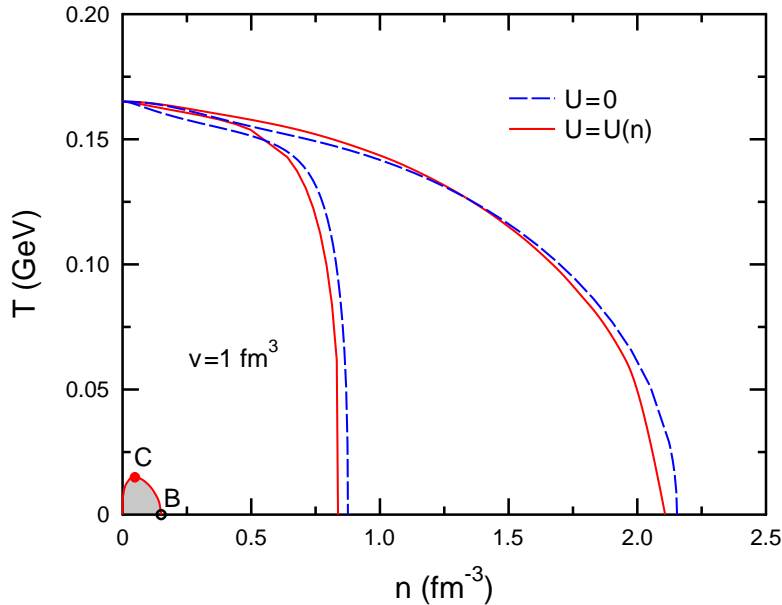


FIG. 31: Same as Fig. 30 but in the $n - T$ plane. Shading shows the region of the LG phase transition.

at $T \sim 100$ MeV. Such a strong phase transition should certainly lead to clear observable signals, e.g. the formation of quark–gluon droplets at final stages of the relativistic nuclear collisions [50, 51].

The condition of zero net strangeness has been imposed in our calculations. It leads to almost linear relation between the strange and baryon chemical potentials. It is shown that the Bose condensation of K^+ mesons is not possible at realistic values of v . We have demonstrated the possibility of the strangeness–antistrangeness separation in the mixed phase. This effect may help to produce clusters of strange matter like strangelets [52, 53] or MEMOS [54] in relativistic heavy-ion collisions. We have calculated the adiabatic trajectories ($S/B = \text{const}$) and found that they have a zigzag-like shape in the mixed phase region. According to our analysis, sometimes the model predicts acausal states ($c_s > 1$), but they lie outside the region reachable in ultrarelativistic heavy-ion collisions. By implementing the mean-field potential for baryons we have described simultaneously the liquid-gas and deconfinement phase transitions. However, properties of the quark-hadron mixed phase are only slightly influenced by the mean-field effects.

In the future we are going to generalize this model by introducing different excluded volumes for different hadronic species. Some attempts in this direction have been already

made in Refs. [18, 21, 55]. Our present approach does not take into account modifications of particle properties in a dense medium, although hadronic masses and radii may significantly change as compared to their vacuum values. This problem should be also studied in the future.

Acknowledgments

The authors thank M.I. Gorenstein for numerous fruitful discussions. We are also grateful to M. Bleicher, M. Hauer, Yu.B. Ivanov, A.V. Merdeev, V.N. Russkikh and G. Torrieri for the interest to this work. L.M.S. acknowledges the kind hospitality and financial support from FIAS. This work was supported in part by the GSI, the DFG grant 436 RUS 113/957/0-1 (Germany), the grants NS-3004.2008.2 and RFFI 09-02-91331 (Russia).

APPENDIX A: THERMODYNAMIC FUNCTIONS OF HADRONIC SYSTEM

In the case of fermions ($B_i = \pm 1$) one can represent the integrals in Eq. (16) in the form [12] which makes easier their numerical calculation at low temperatures:

$$\begin{pmatrix} \tilde{\epsilon}_i \\ P_i \\ \tilde{n}_i \end{pmatrix} = \frac{g_i}{2\pi^2} \int_{m_i}^{\infty} d\epsilon \frac{\sqrt{\epsilon^2 - m_i^2}}{e^{\frac{\epsilon - \tilde{\mu}_i}{T}} + 1} \operatorname{sgn}(\epsilon - \tilde{\mu}_i) \begin{pmatrix} \epsilon^2 \\ \frac{1}{3}(\epsilon^2 - m_i^2) \\ \epsilon \end{pmatrix} + \frac{g_i}{2\pi^2} \begin{pmatrix} \frac{p_F^4}{4} \psi\left(\frac{m_i}{p_F}\right) \\ \frac{\tilde{\mu}_i p_F^3}{3} - \frac{p_F^4}{4} \psi\left(\frac{m_i}{p_F}\right) \\ \frac{p_F^3}{3} \end{pmatrix} \Theta(\tilde{\mu}_i - m_i). \quad (\text{A.1})$$

Here $p_F = \sqrt{\tilde{\mu}_i^2 - m_i^2}$, $\Theta(x) = \frac{1}{2}(1 + \operatorname{sgn}x)$ and $\psi(x)$ is defined as

$$\psi(x) = 4 \int_0^1 dt t^2 \sqrt{t^2 + x^2} = \left(1 + \frac{x^2}{2}\right) \sqrt{1 + x^2} - \frac{x^4}{2} \ln \frac{1 + \sqrt{1 + x^2}}{x}. \quad (\text{A.2})$$

The integrals in the first term of Eq. (A.1) vanish at $T \rightarrow 0$. They were calculated numerically using the Newton-Cotes method.

In the case of mesons ($B_i = 0$) we calculate integrals in Eq. (16) by representing them as series of modified Bessel functions:

$$\begin{pmatrix} \tilde{\epsilon}_i \\ P_i \\ \tilde{n}_i \end{pmatrix} = \frac{g_i m_i^3}{2\pi^2} \sum_{l=1}^{\infty} \exp\left(\frac{\tilde{\mu}_i l}{T}\right) \begin{pmatrix} \frac{m_i}{x} \left(K_1 + \frac{3K_2}{x}\right) \\ \frac{m_i K_2}{x^2} \\ \frac{K_2}{x} \end{pmatrix}, \quad (\text{A.3})$$

where $x = m_i l/T$ and $K_n = K_n(x)$ is the MacDonal function of the n -th order. These series converge if $\tilde{\mu}_i < m_i$ (see first footnote on page 6).

-
- [1] F. Karsch, E. Laermann, and A. Peikert, Nucl. Phys. B **605**, 579 (2001).
 - [2] M. Gyulassy and L. McLerran, Nucl. Phys. A **750**, 30 (2004).
 - [3] P. de Forcrand and O. Philipsen, JHEP **01**, 077 (2007).
 - [4] M.G. Alford, K. Rajagopal, and F. Wilczek, Phys. Lett. B **422**, 247 (1998).
 - [5] O. Scavenius, A. Mocsy, I.N. Mishustin, and D.H. Rischke, Phys. Rev. C **64**, 045202 (2001).
 - [6] I.C. Arsene, L.V. Bravina, W. Cassing, Yu.B. Ivanov, A. Larionov, J. Randrup, V.N. Russkikh, V.D. Toneev, G. Zeeb, and D. Zschesche, Phys. Rev. C **75**, 034902 (2007).
 - [7] S.V. Afanasiev et al. (NA49 Collaboration), Phys. Rev. C **66**, 054902 (2002).
 - [8] C. Alt et al. (NA49 Collaboration), Phys. Rev. C **77**, 024903 (2008).
 - [9] I.N. Mishustin, L.M. Satarov, H. Stöcker, and W. Greiner, Phys. Rev. C **66**, 015202 (2002).
 - [10] U. Heinz, P.R. Subramanian, H. Stöcker, and W. Greiner, J. Phys. G **12**, 1237 (1986).
 - [11] J.D. Walecka, Ann. Phys. **83**, 491 (1974).
 - [12] L.D. Landau and E.M. Lifshitz, *Statistical physics*, Pergamon Press, 1980.
 - [13] R. Hagedorn and J. Rafelski, Phys. Lett. **97B**, 136 (1980).
 - [14] F. Karsch and H. Satz, Phys. Rev. D **21**, 1168 (1980).
 - [15] J.I. Kapusta, Phys. Rev. D **23**, 2444 (1981).
 - [16] D.H. Rischke, M.I. Gorenstein, H. Stöcker, and W. Greiner, Z. Phys. C **51**, 485 (1991).
 - [17] R. Veugopalan and M. Prakash, Nucl. Phys. A **546**, 718 (1992).
 - [18] G.D. Yen, M.I. Gorenstein, W. Greiner, and S.N. Yang, Phys. Rev. C **56**, 2210 (1997).
 - [19] S. Wheaton and J. Cleymans, hep-ph/0407174.
 - [20] C. Greiner, P. Koch, and H. Stöcker, Phys. Rev. Lett. **58**, 1825 (1987).
 - [21] M.I. Gorenstein, M. Gaździcki, and W. Greiner, Phys. Rev. C **72**, 024909 (2005).
 - [22] Particle Data Group, C. Amsler et al., Phys. Lett. B **667**, 1 (2008).
 - [23] D.B. Kaplan and A.E. Nelson, Phys. Lett. B **175**, 57 (1986).
 - [24] J. Schaffner, A. Gal, I.N. Mishustin, H. Stöcker, and W. Greiner, Phys. Lett. B **334**, 268 (1994).
 - [25] J. Schaffner, J. Bondorf, and I.N. Mishustin, Nucl. Phys. A **625**, 325 (1997).
 - [26] I. Zakout, W. Greiner, and H.R. Jaqaman, Nucl. Phys. A **759**, 201 (2005).
 - [27] J. Cleymans and H. Satz, Z. Phys. C **57**, 135 (1993).
 - [28] P. Braun–Munzinger, and J. Stachel, Nucl. Phys. A **606**, 320 (1996).
 - [29] A. Andronic, P. Braun–Munzinger, and J. Stachel, ArXiv: 0812.1186 [nucl-th].
 - [30] L. Ahle et al. (E866/E917 Collaboration), Phys. Lett. B **476**, 1 (2000).
 - [31] B.I. Abelev et al. (STAR Collaboration), ArXiv: 0808.2041 [nucl-ex].
 - [32] C. Pinkenburg et al. (E895 Collaboration), Nucl. Phys. A **698**, 495 (2002).

- [33] S. Albergo et al. (E896 Collaboration), Phys. Rev. Lett. **88**, 062301 (2002).
- [34] F. Becattini, M. Gaździcki, A. Keränen, J. Manninen, and R. Stock, Phys. Rev. C **69**, 024905 (2004).
- [35] Yu.B. Ivanov, A.S. Khvorostukhin, E.E. Kolomeitsev, V.V. Skokov, V.D. Toneev, and D.N. Voskresensky, Phys. Rev. C **72**, 025804 (2005).
- [36] L.M. Satarov, I.N. Mishustin, A.V. Merdeev, and H. Stöcker, Phys. Rev. C **75**, 024903 (2007).
- [37] L.M. Satarov, I.N. Mishustin, A.V. Merdeev, and H. Stöcker, Yad. Fiz. **70**, 1822 (2007) [Phys. Atom. Nucl. **70**, 1773 (2007)].
- [38] D. Teaney, J. Lauret, and E.V. Shuryak, Phys. Rev. Lett. **86**, 4783 (2001).
- [39] L.D. Landau and E.M. Lifshitz, *Fluid Mechanics*, Pergamon Press, 1987.
- [40] A. Andronic, P. Braun–Munzinger, and J. Stachel, Nucl. Phys. A **772**, 167 (2006).
- [41] I.N. Mishustin, L.M. Satarov, H. Stöcker, and W. Greiner, Yad. Fiz. **64**, 866 (2001) [Phys. Atom. Nucl. **64**, 802 (2001)].
- [42] J. Cleymans and K. Redlich, Phys. Rev. Lett. **81**, 5284 (1998).
- [43] K. Paech, M. Reiter, A. Dumitru, H. Stöcker, and W. Greiner, Nucl. Phys. A **681**, 41 (2001).
- [44] W. Trautmann, Nucl. Phys. A **752**, 407 (2005).
- [45] T.H.R. Skyrme, Phil. Mag. **1**, 1043 (1956); Nucl. Phys. **9**, 615 (1959).
- [46] G. Sauer, H. Chandra, and U. Mosel, Nucl. Phys. A **264**, 221 (1976).
- [47] J.P. Bondorf, A.S. Botvina, A.S. Iljinov, I.N. Mishustin, and K. Sneppen, Phys. Rep. **257**, 133 (1995).
- [48] J. Pochodzalla et al., Phys. Rev. Lett. **75**, 1040 (1995).
- [49] P. Chomaz, M. Colonna, and J. Randrup, Phys. Rep. **389**, 263 (2004).
- [50] I.N. Mishustin, Phys. Rev. Lett. **82**, 4779 (1999).
- [51] G. Torrieri, B. Tomasik, and I.N. Mishustin, Phys. Rev. C **77**, 034903 (2008).
- [52] S.A. Chin and A.K. Kerman, Phys. Rev. Lett. **43**, 1292 (1979).
- [53] E. Farhi and R.L. Yaffe, Phys. Rev. D **30**, 2379 (1984).
- [54] J. Schaffner, C. Greiner, and H. Stöcker, Phys. Rev. C **46**, 322 (1992).
- [55] M.I. Gorenstein, A.P. Kostyuk, and Ya.D. Krivenko, J. Phys. G **25**, L75 (1999).
- [56] As claimed in Ref. [14], crystallization into a solid state should occur at densities near the close packing limit $n_{\text{cp}} = (4\sqrt{2}r_h^3)^{-1} \simeq 3v^{-1}$. Our estimates show, however, that a dense hadronic system should earlier undergo the transition into a quark–gluon phase.
- [57] In Eq. (16) we assume that the condition of Bose–condensation $\tilde{\mu}_i > m_i$ is not satisfied (see below).
- [58] Except of $f_0(600)$, a very similar set of hadrons has been used in the THERMUS thermal model [19].
- [59] For the observed decay channels with unknown probabilities we assume equal branching ratios.
- [60] Here we disregard possible in-medium modifications of meson properties. This question have been studied on the mean field level in Refs. [24, 25, 26].

- [61] Using the isospin symmetry we write $K^+/\pi^+ = 1.5n_K^*/n_\pi^*$.
- [62] The factor $2/3$ comes from a naive consideration based on the $SU(3)$ flavor symmetry.
- [63] As was mentioned on page 8, $\mu \sim \frac{1}{2}\mu_S$, so that $\mu - \mu_S \sim \mu_S$.
- [64] For simplicity it is assumed that strange and nonstrange baryons have the same mean-field potentials. On the other hand, in the considered case of chemically equilibrated matter with zero strangeness, the medium-range interactions are not so important at high temperatures $T \gtrsim 100$ MeV, when the abundances of hyperons, antibaryons and mesons become significant.